Published in final edited form as:

Cell Rep. 2020 October 27; 33(4): 108321. doi:10.1016/j.celrep.2020.108321.

Fat body p53 regulates systemic insulin signaling and autophagy under nutrient stress via *Drosophila* Upd2 repression

María Clara Ingaramo[1], **Juan Andrés Sánchez**[1], **Norbert Perrimon**[3,4,*], **Andrés Dekanty**[1,2,5,*]

[1]Instituto de Agrobiotecnología del Litoral, Consejo Nacional de Investigaciones Cientificas y Técnicas (CONICET), Santa Fe, 3000, Argentina

[2]Facultad de Bioquímica y Ciencias Biólogicas, Universidad Nacional del Litoral (UNL), Santa Fe, 3000, Argentina

[3]Department of Genetics, Blavatnik Institute, Harvard Medical School, Boston, MA 02115, USA

[4]Howard Hughes Medical Institute, Boston, MA 02115, USA

[5]Lead Contact

SUMMARY

The tumor suppressor p53 regulates multiple metabolic pathways at the cellular level. However, its role in the context of a whole animal response to metabolic stress is poorly understood. Using *Drosophila*, we show AMPK-dependent Dmp53 activation is critical for sensing nutrient stress, maintaining metabolic homeostasis and extending organismal survival. Under both nutrient deprivation and high-sugar diet, Dmp53 activation in the fat body represses expression of the *Drosophila* Leptin analog, Unpaired-2 (Upd2), which remotely controls Dilp2 secretion in insulin-producing cells. In starved Dmp53-depleted animals, elevated Upd2 expression in adipose cells and activation of Upd2 receptor Domeless in the brain result in sustained Dilp2 circulating levels and impaired autophagy induction at a systemic level, therefore reducing nutrient stress survival. These findings demonstrate an essential role for AMPK-Dmp53 axis in nutrient stress responses and expand the concept that adipose tissue acts as a sensing organ that orchestrate systemic adaptation to nutrient status.

Graphical Abstract

*Correspondence: Andrés Dekanty, adekanty@santafe-conicet.gov.ar, Phone/Fax: +54 342 4511370 int. 5022; Norbert Perrimon, perrimon@genetics.med.harvard.edu, Phone/Fax: +1 617 432-7672.

Author Contributions

M.C.I. designed and performed experiments, analyzed data, and edited the manuscript. J.A.S. performed experiments. N.P. participated in experimental design and edited the manuscript. A.D. designed experiments, analyzed data, and wrote the manuscript.

Declaration of interests

The authors declare no competing interests.

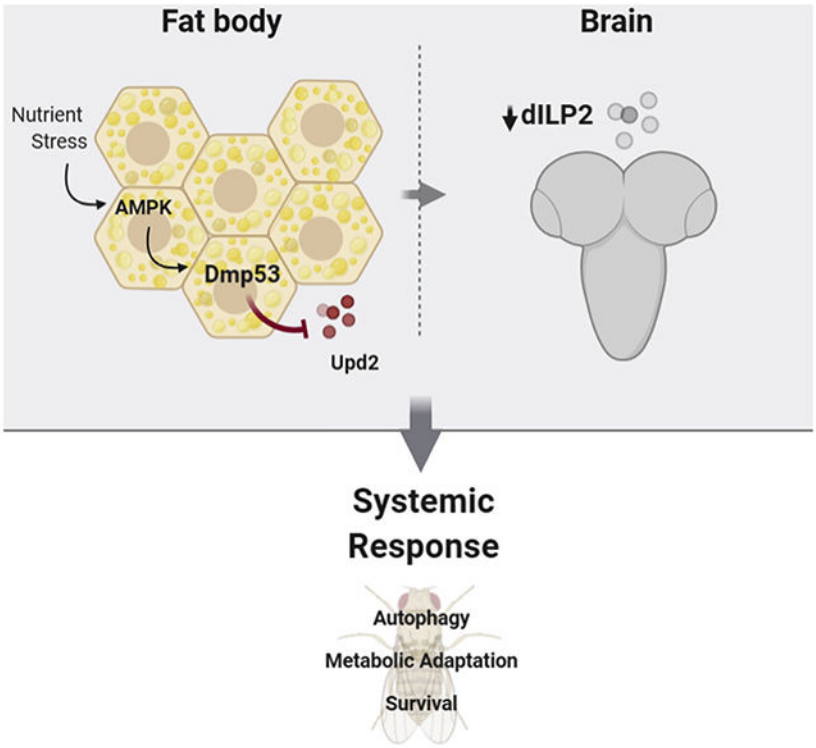

Keywords

Drosophila ; p53; AMPK; Upd2/Leptin; insulin-producing cells; fat body; metabolism

INTRODUCTION

The ability of an organism to sense nutrient stress and coordinate metabolic and physiological responses is critical for its survival. Over the last years, the p53 tumor suppressor has emerged as an important regulator of cellular metabolism and its activation has been regularly observed in response to diverse metabolic inputs such as changes in oxygen levels or nutrient availability (Berkers et al., 2013). It has been shown that p53 interacts with main players in key nutrient sensing pathways such as mammalian target of rapamycin (mTOR) and AMP-activated protein kinase (AMPK), leading to modulation of autophagy and lipid and carbohydrate metabolism. p53 restricts tumor development partially by inhibiting glycolysis (Zawacka-Pankau et al., 2011), limiting the pentose phosphate pathway (Jiang et al., 2011) and promoting mitochondrial respiration (Berkers et al., 2013; Liang et al., 2013). Conversely, p53 activation can benefit tumor growth by stimulating adaptive cellular responses in nutrient-deficient conditions. p53 activation is known to induce cell-cycle arrest and promote cell survival in response to transient glucose deprivation (Jones et al., 2005), regulate autophagy and increase cell fitness upon fasting (Scherz-Shouval et al., 2010), and promote cancer cell survival and proliferation after serine or glutamine depletion (Maddocks et al., 2013; Tajan et al., 2018). Therefore, p53 plays a pivotal role in the ability of cells to sense and respond to nutrient stress, functions that are important not only to control cancer development but also to regulate crucial aspects of

animal physiology. Further studies concerning p53 regulation and function in response to nutrient and metabolic challenges at an organismal level would expand our understanding on the role of p53 in normal animal physiology, aging and disease.

The single *Drosophila* ortholog of mammalian p53 (Dmp53) has also been shown to regulate tissue and metabolic homeostasis (Barrio et al., 2014; Contreras et al., 2018; Ingaramo et al., 2018; Mesquita et al., 2010; Sanchez et al., 2019). Dmp53 regulates energy metabolism through induction of cell-cycle arrest and cell growth inhibition in response to mitochondrial dysfunction (Mandal et al., 2010) by regulating glycolysis and oxidative phosphorylation to promote cell fitness in dMyc overexpressing cells (De La Cova et al., 2014) and by modulating autophagy protecting the organism from oxidative stress (Robin et al., 2019). Studies in *Drosophila* have also identified tissue specific roles of Dmp53 in regulating lifespan and adaptive metabolic responses impacting on animal aging and stress survival (Barrio et al., 2014; Bauer et al., 2007; Hasygar and Hietakangas, 2014; Robin et al., 2019), evidencing conserved functions of p53 (Liu et al., 2017, 2014) and positioning *Drosophila* p53 studies as a valuable alternative providing relevant insights on mammalian health and disease.

The insulin pathway is highly conserved from mammals to *Drosophila* and regulates carbohydrate and lipid metabolism, tissue growth, and longevity in similar ways (Taguchi and White, 2008; Wu and Brown, 2006). *Drosophila* insulin-like peptides (Dilp) promote growth and maintain metabolic homeostasis through activation of a unique insulin receptor (dInR) and of a conserved intracellular insulin and IGF signaling pathway (IIS) (Andersen et al., 2013; Ikeya et al., 2002). Dietary conditions tightly regulate Dilp2 production and/or secretion from the insulin-producing cells (IPCs), neuroendocrine cells analogous to pancreatic β-cells located in the fly brain (Ikeya et al., 2002; Rulifson et al., 2002). Interestingly, a nutrient sensing mechanism in the fat body (FB), a functional analog of vertebrate adipose and hepatic tissues, non-autonomously regulates Dilp2 secretion and couples systemic growth and metabolism with nutrient availability (Géminard et al., 2009). According to the nutritional status, the FB produces signaling molecules capable of promoting or inhibiting insulin secretion from the IPCs (Agrawal et al., 2016; Delanoue et al., 2016; Koyama and Mirth, 2016; Meschi et al., 2019; Rajan and Perrimon, 2012; Sano et al., 2015). Thus, a simple integrated system composed of various organs and conserved signaling pathways regulates metabolic homeostasis and organismal growth in response to nutrient availability.

The FB also functions as the organism’s main energy reserve and is responsible for coupling energy expenditure to nutrient status (Arrese and Soulages, 2010). In well-fed animals, circulating insulin activates insulin receptors in the FB and promotes energy storage in the form of glycogen and triacylglycerol (TAG). Upon limited nutrient availability, stored lipids and glycogen are broken down to supply energy for the rest of the body (Arrese and Soulages, 2010). In previous work, we showed that FB-specific inhibition of Dmp53 activity accelerated the consumption of main energy stores, reduced sugar levels and compromised organismal survival during nutrient deprivation (Barrio et al., 2014). The mechanism by which Dmp53 regulates metabolic homeostasis and organismal survival under nutrient stress

is not entirely understood and might involve regulation of specific signaling and metabolic pathways.

Here, we provide evidence that AMPK-dependent Dmp53 activation in the FB non-cell-autonomously regulates TOR signaling and autophagy induction upon acute starvation which is essential for organismal survival. Dmp53 activation in response to nutritional stress is required for proper communication between the FB and IPCs by modulating the expression of the *Drosophila* Leptin analog, Unpaired-2 (Upd2). Elevated Upd2 levels in adipose cells of starved Dmp53-depleted animals result in sustained Dilp2 circulating levels, activation of insulin/TOR signaling and impaired autophagy induction in the whole animal, therefore reducing survival rates upon nutrient deprivation. These results indicate that Dmp53 plays an essential role in *Drosophila* integrating nutrient status with metabolic homeostasis by modulating Dilp2 circulating levels, systemic insulin signaling and autophagy.

RESULTS

Fat body Dmp53 activity regulates organismal resistance to challenging nutrient conditions

To better understand the role of Dmp53 in metabolic homeostasis and nutrient stress response, we sought to analyze the impact of FB specific inhibition of Dmp53 transcriptional activity on organismal survival upon different nutrient conditions. To specifically reduce Dmp53 activity in the FB we expressed a dominant negative version of Dmp53 lacking DNA-binding activity (Dmp53$^{H159.N}$) under the control of the FB *cg-Gal4* driver (referred to as *cg>p53$^{H159.N}$*). When maintained on a normal diet, *cg>p53$^{H159.N}$* larvae exhibited slight change or no difference in pupal size, TAG level, glycogen content, and circulating glucose compared to control flies (Fig. S1 and (Barrio et al., 2014)). Upon starvation, *cg>p53$^{H159.N}$ and cg>p53^{RNAi}* adult flies exhibited a clear reduction in survival rates accompanied by an accelerated rate of glycogen consumption as reported in previous work (Fig. 1A,B, S1 and (Barrio et al., 2014)). Similarly, 4h starvation treatment of mid-third instar larvae (mid-L3) led to a rapid decrease in glycogen content in *cg>p53$^{H159.N}$* larvae compared to control animals (Fig. 1B), indicating that Dmp53 is playing a role in the short-term starvation response both in larval and adult stages. Consistent with this, Dmp53 is activated upon acute starvation as shown by increased expression of a Dmp53 activity reporter (*p53^{RE}-GFP*, consisting in p53 consensus DNA binding sites driving GFP expression; (Barrio et al., 2014; Lu et al., 2010)) following a 4h starvation treatment (Fig. 1C). Interestingly, high-sugar diet (HSD)-fed animals presented higher *p53^{RE}-GFP* levels which can be blocked by Dmp53$^{H159.N}$ expression (Fig. 1D), and *cg>p53$^{H159.N}$* larvae showed a strong developmental delay and reduced viability on HSD when compared to control animals (Fig. 1E and S1), which suggests a general role of Dmp53 in maintaining metabolic homeostasis under nutrient stress. Together, these results indicate that Dmp53 is activated in FB cells exposed to acute starvation and HSD treatments and that Dmp53 activation in FB is required for maintaining metabolic homeostasis and promoting survival. Therefore, despite Dmp53 absence in the FB appears to have minor effects on metabolism

under normal diet, it plays a critical role in regulating energetic homeostasis and organismal survival under different nutritional stress conditions.

Fat body Dmp53 activity is required to reduce TOR signaling and induce autophagy under nutrient deprivation

As the TOR pathway is a common regulator of energy metabolism, we explored the effects of depleting Dmp53 activity in the FB on TOR pathway activity. We first measured phosphorylation of S6 kinase, a well-described downstream target of TOR activity by western blot using a phospho-*Drosophila* p70 S6 kinase (Thr398) antibody. Starvation treatment of midL3 larvae led to a rapid decrease in TOR-dependent phosphorylation of S6K (p-S6K) in FB extracts (Fig. 2A). Expression of $Dmp53^{H159.N}$ under the control of the *cg-Gal4* driver showed higher levels of p-S6K in FB samples of starved animals (Fig. 2A). We also analyzed *unk* gene expression which is induced after TORC1 inhibition (Tiebe et al., 2015; Fig. 2B) and observed reduced induction of endogenous *unk* transcript levels in Dmp53-depleted FBs (Fig. 2B), strongly suggesting that TOR signaling is maintained more actively in starved Dmp53-depleted animals. To investigate how sustained TORC1 signaling impacts on autophagy induction in starved *cg>p53*$^{H159.N}$ animals we used either a transgenic autophagy reporter, mCherry-tagged-Atg8a (mChAtg8), or the cell-permeable Lysotracker dye, which target acidic organelles including autolysosomes. A clear accumulation of Lysotracker-positive vesicles was observed in FB cells of wild-type larvae following 4h of starvation (Fig. 2C). Interestingly, starvation-induced autophagy was strongly reduced in *dmp53* mutant animals (*dmp53*^{ns} and *dmp53*^{5A14}; Fig. 2C) or when expressing Dmp53 dominant negative versions ($Dmp53^{H159.N}$, $Dmp53^{259.N}$ and $Dmp53^{R155H}$) under *cg-Gal4* control (Fig. 2C–E). Since *cg-Gal4* is mainly expressed in FB cells as well as lymph gland and haemocytes, we analyzed autophagy induction upon depletion of Dmp53 activity in the FB by using complementary Gal4 lines. $Dmp53^{H159.N}$ expression under the control of *lpp, ppl, R4* and *Lsp2* Gal4 drivers strongly reduced starvation-induced autophagy (Fig. 2E and S2). Similar results were obtained with *cg-Gal4* in combination with *elav-Gal80*, which prevents expression of UAS-transgenes in most parts of the brain (Fig. S2). In contrast, salivary gland- or brain-specific depletion of Dmp53 activity (using *SG-Gal4, fkh-Gal4, elav-Gal4* and *dilp2-Gal4)* did not have any impact on starvation-induced autophagy (Fig. S2). Starvation treatment also showed accumulation of mChAtg8 positive autophagosomes and autolysosomes all through the larval FB that was suppressed in *dmp53*^{5A14} animals or by $Dmp53^{H159.N}$ expression (Fig. 2F and S2). Note that following long-term starvation (16h) $Dmp53^{H159.N}$ expressing FBs showed accumulation of mChAtg8 positive vesicles, pointing to a defect in short-term starvation response mechanisms (Fig. S2). Collectively, these results indicate that Dmp53 activity in the FB regulates TOR activity and autophagy induction upon acute nutrient deprivation.

Next, we asked whether impaired autophagy is responsible for reduced survival rates of *cg>p53*$^{H159.N}$ animals exposed to starvation. Chloroquine (CQ) inhibits autophagy as it raises lysosomal pH, leading to inhibition of both autophagosome-lysosome fusion and lysosomal protein degradation. Interestingly, whereas CQ treatment renders flies more sensitive to starvation at a similar extent as *cg>p53*$^{H159.N}$ (Fig. 2G), it did not increase sensitivity to starvation of *cg>p53*$^{H159.N}$ flies. Similar results were obtained when blocking

autophagy induction in the FB by expression of $ATG1^{RNAi}$ (Fig. S2), strongly suggesting that inhibition of autophagy contributes to the reduced survival rates of starved, Dmp53-depleted animals. We then used rapamycin, a potent inhibitor of TOR signaling, to test whether reducing TOR activity would affect survival rates of Dmp53-depleted animals to starvation. Rapamycin treatment significantly increased starvation resistance of control and *cg>p53*$^{H159.N}$ adult flies (Fig. 2I) and partially rescued autophagy induction (Fig. 2H and S2), indicating that sustained TOR activity contributes to the reduced survival rates of starved, Dmp53-depleted animals. Altogether, these data indicate that Dmp53 activation in FB of starved animals is required to reduce TOR signaling, induce autophagy and promote starvation resistance.

Fat body Dmp53 non-cell-autonomously regulates TOR signaling and autophagy induction upon starvation

Autophagy induction is inhibited by TOR, which is activated both by insulin signaling and directly by nutrients (Rusten et al., 2004; Scott et al., 2004). We then asked whether Dmp53 plays a cell autonomous or non-autonomous function in regulating starvation-induced autophagy. Notably, expression of $Dmp53^{H159.N}$ in single FB cells by using the actin-flip-out-Gal4 technique was unable to impair autophagy induction following 4h starvation treatment (Fig. 3A; compare mChATG8 accumulation in control (GFP^{-}) and $Dmp53^{H159.N}$ (GFP^{+}) expressing cells). Next, we analyzed expression of the *unk-lacZ* transcriptional reporter that bears a dimerized enhancer region from *unk* intron 2, which is strongly induced after TORC1 inhibition (Tiebe et al., 2015 and Fig. 3C). Upregulation of *unk-lacZ* in the FB of starved animals was significantly reduced when expressing $Dmp53^{H159.N}$ under *cg-Gal4* control (Fig. 3C). Interestingly, however, starvation-induced *unk-lacZ* expression was not affected when blocking Dmp53 activity in single FB cells (Fig. 3B), strongly suggesting that Dmp53 influences TOR signaling and autophagy induction in a cell-non-autonomous manner. We also analyzed the level of expression of upstream TOR elements, such as TSC2 and Sirtuins, along with several Autophagy-related genes (Atg) and found no significant differences between *cg>p53*$^{H159.N}$ and controls (Fig. S3). To confirm that FB Dmp53 has an impact on systemic autophagy induction, we examined Lysotracker staining in other tissues different from the FB. Interestingly, while we observed a significant increase in Lysotracker positive puncta in brain, salivary gland and intestine of starved control animals, autolysosomes were almost completely absent in these tissues upon expression of $Dmp53^{H159.N}$ in the FB (Fig. 3D). Altogether, these findings point to a tissue-specific role of *Drosophila* p53 in regulating systemic TOR signaling and autophagy induction upon fasting.

Dmp53 activation in the fat body is required to reduce Dilp2 circulating levels and systemic insulin signaling

As stated before, TOR activity and autophagy induction can be modulated directly by nutrients as well as by insulin signaling (Scott et al., 2004; Rusten et al., 2004), and the FB integrates nutritional inputs with Dilp2 secretion at the IPCs (Géminard et al., 2009). To study a possible function of FB Dmp53 in controlling systemic insulin signaling, we analyzed Dilp2 protein levels in IPCs upon fasting. As previously described, starvation treatment led to a rapid accumulation of Dilp2 protein in IPCs of control animals (Fig. 4A). Expression of $Dmp53^{H159.N}$ in the FB, however, resulted in significantly less Dilp2

accumulation upon acute starvation treatment (Fig. 4A). Note that similarly to what is seen with autophagy, following long-term starvation treatment (24h) *cg>p53$^{H159.N}$* animals showed similar Dilp2 protein levels in the IPCs than controls (Fig. S4). To confirm IPCs Dilp2 retention, we measured epitope-tagged Dilp2 levels (Dilp2HF)(Park et al., 2014) in hemolymph of starved control and Dmp53-depleted animals by ELISA. Whereas no differences were observed between genotypes in well fed conditions (Fig. S4), elevated levels of circulating insulin were observed in starved *cg>p53$^{H159.N}$* animals (Fig. 4B). Note that we found no significant difference in *dilp2 and dilp5* transcript levels between control and Dmp53-depleted larvae in either well fed or starved conditions (Fig. S4).

To assess whether sustained Dilp2 circulating levels in starved Dmp53-depleted animals has an impact on systemic insulin signaling, we first measured *4EBP* and *dInR* transcript levels. These two genes are direct transcriptional targets of dFOXO (Puig et al., 2003; Teleman et al., 2005), which is negatively regulated by the insulin pathway. Consistent with a rapid drop of circulating Dilp2, *4EBP* and *dInR* transcript levels were strongly induced in control larvae upon nutrient deprivation (Fig. 4C). Interestingly, however, starvation-induced expression of these genes was significantly reduced in *cg>p53$^{H159.N}$* larvae (Fig. 4C). Additionally, we used the tGPH reporter for *in vivo* PI3K activity, which consists of a GFP-Pleckstrin Homology domain fusion protein ubiquitously expressed under the control of *β-tubulin* promoter. tGPH is localized to plasma membrane in FB and salivary gland cells of well-fed animals (Fig. S4 and (Britton et al., 2002)). In contrast, membrane-associated tGPH is diminished under nutrient deprivation as a consequence of reduced insulin signaling (Fig. 4D and (Britton et al., 2002)). Impairing Dmp53 transcriptional activity specifically in the FB showed higher tGPH levels at the plasma membrane of starved mid-L3 larvae than control animals (Fig. 4D). Consistent with a non-cell autonomous role of Dmp53 in regulating systemic insulin signaling, these results were observed in cells from both FB and salivary gland (Fig. 4D), and expression of Dmp53$^{H159.N}$ in single FB cells did not affect tGPH localization following 4h starvation treatment (Fig. 4E; compare membrane-associated tGPH levels in control (RFP^{-}) and Dmp53$^{H159.N}$ (RFP^{+}) expressing cells).

Next, we evaluated to what extent the increased Dilp2 circulating levels observed in starved Dmp53 depleted animals were responsible for their reduced survival rates. Overexpression of ImpL2, a secreted protein that binds Dilp2 and inhibits insulin receptor signaling in a non-cell-autonomous manner, completely reverted the starvation sensitivity caused by Dmp53 activity depletion in the FB (Fig. 4F). Additionally, ImpL2 overexpression reverted autophagy induction kinetics in starved *cg>p53$^{H159.N}$* animals (Fig. 4G and S4). Importantly, IPCs-specific depletion of Dmp53 activity (using *dilp2-Gal4*) did not have any impact on either starvation sensitivity (Fig. S4) or autophagy induction (Fig. S2). Taken together, these results indicate that Dmp53 activity in the FB of starved animals reduces Dilp2 circulating levels, therefore influencing systemic insulin and TOR signaling, autophagy induction and starvation resistance.

Dmp53-dependent regulation of Unpaired-2 influences Dilp2 levels, autophagy induction and organismal survival upon nutrient stress

Communication between the FB and the brain relies on humoral signals emitted by fat cells according to nutrient conditions (Britton and Edgar, 1998; Géminard et al., 2009). To further understand the role of Dmp53 in brain-FB intercommunication and the nature of the signals involved, we set up *ex vivo* experiments. Inverted larvae from control (*cg>GFP*) and *cg>Dmp53*$^{N159.H}$ animals were incubated in M3 insect medium (equivalent to starvation treatment, (Kim and Neufeld, 2015)) and stained to visualize IPCs Dilp2 levels. Recapitulation of Dilp2 secretion results obtained *in vivo* was evidenced by rapid increase in IPCs Dilp2 levels after 3h incubation of control inverted larvae in M3 medium compared with inverted larvae at the time of dissection (WF; Fig. 5A). Inverted larvae from *cg>Dmp53*$^{N159.H}$ animals showed significantly less Dilp2 accumulation (Fig. 5A). As FB secreted molecules have been described acting either positively or negatively on Dilp2 secretion, we then intended to distinguish between these two possibilities by performing *ex vivo* co-culture experiments in which inverted larvae from control and *cg>Dmp53*$^{N159.H}$ animals were incubated together. Interestingly, Dilp2 accumulation levels in the IPCs of control larvae were drastically reduced when co-cultured with *cg>Dmp53*$^{N159.H}$ inverted larvae (Fig. 5A, compare middle and right panel; see also Fig. 5B for quantifications of Dilp2 intensity levels). Similar results were obtained when dissected brains from control mid-L3 larvae were cultured in M3 medium in the presence of isolated control or Dmp53-depleted fat bodies (Fig. 5C,D). As a physiological readout of insulin/TOR signaling, we also monitored induction of autophagy in *ex vivo* experiments. Whereas *ex vivo* incubation of inverted larvae in M3 medium led to a rapid accumulation of mChATG8 positive vesicles throughout wild type larval FB, co-cultures of inverted larvae from wild-type and Dmp53-depleted animals prevented autophagy induction (Fig. S5). Altogether, these series of *ex vivo* experiments point to an overproduction of secreted molecules that stimulate Dilp2 secretion by Dmp53-depleted fat bodies under starvation conditions.

Next, we analyzed the expression of genes encoding FB secreted molecules known to regulate Dilp2 secretion such as Upd2, CCHa1, CCHa2, GBP1, GBP2 and Sun. qRT-PCR analysis showed significant differences in *upd2* and *sun* transcript levels between controls and *cg>p53*$^{H159.N}$ larvae exposed to a 4h starvation treatment (Fig. 6A). In contrast, no differences were observed for *ccha1, ccha2, gbp1* and *gbp2* mRNA levels (Fig. 6A). Thus, we conducted a candidate screen in which these adipokines were specifically silenced in the FB of larvae either well fed or exposed to starvation and screened for their capacity to recover autophagy induction in *cg>p53*$^{H159.N}$ animals. Strikingly, *upd2*^{i} expression in the FB was able to rescue the autophagy delay observed in starved *cg>p53*$^{H159.N}$ animals (Fig. 6B and S6). *Drosophila* cytokine Unpaired 2 (Upd2) has been described as a secreted factor produced by FB cells in well fed animals, mainly responding to dietary fat and sugars (Rajan and Perrimon, 2012). FB-derived Upd2 promotes Dilp2 secretion and systemic growth by activating the Janus kinase (JAK)/Signal Transducer and Activator of Transcription (STAT) signaling pathway in GABAergic neurons (Rajan and Perrimon, 2012). Notably, depletion of *Drosophila* JAK/STAT receptor Domeless (Dome) in GABAergic neurons by expressing *dome*^{i} under *vgat-Gal4* control largely reverted impaired autophagy induction observed in starved, *dmp53*^{5A14} mutant larvae (Fig. 6D and S6).

Consistent with a role of FB Upd2 in modulating insulin secretion, expressing *upd2*^{i} along with Dmp53$^{H159.N}$ showed similar Dilp2 accumulation levels in the IPCs of starved larvae than *upd2*^{i}-expressing larvae (Fig. 6C). We then evaluated at which extent increased Upd2 levels can account for the reduced survival rates observed in starved *cg>p53*$^{H159.N}$ animals. Notably, *upd2*^{i} expression fully rescued starvation sensitivity caused by Dmp53 activity depletion in the FB (Fig. 6E). Similarly, reduced survival rates displayed by *dmp53*^{5A14} mutant flies was restored when reducing *Dome* expression in adult GABAergic neurons (Fig. 6F). Altogether, our results indicate that sustained FB Upd2 expression and activation of JAK/STAT signaling in GABAergic neurons is responsible for increased Dilp2 circulating levels, reduced autophagy induction and hypersensitivity to starvation displayed by Dmp53-depleted animals. Interestingly, recent ChIP-Seq analysis showed Dmp53 binding to Upd2 locus in *Drosophila* embryos and adult heads (Kudron et al., 2018; Kurtz et al., 2019). Considering the identification of a conserved p53 binding site at the same location (Fig. S6), we propose that Dmp53 may directly regulate Upd2 expression in the FB of starved animals.

AMPK-dependent Dmp53 activation regulates systemic insulin signaling and autophagy induction upon nutrient stress

TOR and AMPK kinases play essential roles in nutrient sensing and are important regulators of cell growth and metabolism (Grewal, 2009; Hietakangas and Cohen, 2009). Whereas TOR is regulated in response to amino acid availability, AMPK is modulated by changes in the cellular ATP:AMP ratio. In order to see whether Dmp53 is activated downstream of TOR or AMPK pathways upon acute starvation treatments, we used the Dmp53 activity reporter, *p53*^{RE}*-GFP*. While rapamycin treatment of mid-L3 larvae significantly increased *unk* transcript levels, it was not able to increase *p53*^{RE}*-GFP* expression (Fig. S7). In contrast, starvation-induced *p53*^{RE}*-GFP* was significantly reduced by expression of *AMPKα*^{i} (Fig. 7A). These results prompted us to analyze a possible non-cell-autonomous role of AMPK in controlling autophagy induction upon nutrient deprivation. To determine whether AMPK activity in the FB has an impact on systemic autophagy induction, we examined lysotracker staining in different tissues of starved animals where AMPK was depleted in the FB by expression *AMPKα*^{i} under *cg-Gal4* control *(cg>AMPKα*^{i}). In all tissues analyzed (brain, salivary gland, intestine and FB), depletion of FB AMPK levels almost completely blocked autophagy induction when compared to control animals (Fig. 7B). Additionally, *AMPKα*^{i} expression in single FB cells had no effect on starvation-induced accumulation of mChAtg8 punctae at a cellular level (Fig. S7). Next, we measured epitope-tagged Dilp2 levels (Dilp2HF) in the hemolymph of starved control and *cg>AMPKα*^{i} animals. Starved AMPK-depleted larvae showed higher Dilp2 circulating levels than controls (Fig. 7C), suggesting that FB AMPK activity indirectly influences Dilp2 release from IPCs. Even though *AMPK* mutant flies show high starvation sensitivity (Johnson et al., 2010), the contribution of FB AMPK activity on this phenotype has not been addressed so far. Interestingly, the expression of *AMPKα*^{i} in the FB reduced survival rates of adult flies exposed to starvation conditions at a similar level as *cg>p53*$^{H159.N}$ (Fig. 7D). Flies expressing *AMPKα*^{i} along with Dmp53$^{H159.N}$ showed similar survival rates as flies expressing each transgene individually (Fig. 7D). Together, these results reveal an AMPK-Dmp53 axis acting in the FB to promote starvation resistance.

Next, we analyzed a possible contribution of FB AMPK-p53 signaling in the response to other nutritional stresses. As shown before, HSD-fed animals showed Dmp53 activation (Fig. 1D) and *cg>p53*$^{H159.N}$ larvae exhibited reduced viability when compared to control animals (Fig. 1E and S1). In addition, *AMPK* knockdown in the FB caused reduced viability of HSD-fed animals (Fig. 7E). Notably, *cg>p53*$^{H159.N}$ animals fed with HSD showed increased *Upd2* expression and elevated Dilp2 circulating levels (Fig. 7F,G), suggesting that the role of p53 in nutrient sensing and in the regulation of systemic insulin signaling may be a general response to nutrient stress rather than a specific response to starvation. Even though we cannot rule out the possibility of an additive effect of HSD and Dmp53 inhibition on Upd expression, our results suggest that Dmp53 is acting through an endocrine mechanism similar to the one used in starvation.

It has been previously shown that Dilp3, but not Dilp2, is involved in acute responses to altered sugar levels. Dietary sugar stimulates Dilp3 secretion from the IPCs, which in turn promotes systemic TOR activation and suppresses autophagy in the larval FB (Kim and Neufeld, 2015). Interestingly, however, animals reared on a high-sugar diet develop insulin resistance and show elevated circulating Dilp2 levels (Musselman and Kühnlein, 2018). At which extent, Dilp3 is also playing a role in chronic responses to HSD and whether altered Dilp3 levels can contribute to Dmp53-dependent phenotypes in excess nutrient stress remain to be studied.

DISCUSSION

A role of p53 in organismal resistance to challenging nutrient conditions

Even though progress has been made in understanding p53 metabolic functions at the cellular level, its role in the context of a whole animal response to metabolic stress is poorly understood. Here, we provide evidence that *Drosophila* p53 is critically involved in nutrient sensing and in the orchestration of an organismal response to nutrient stress. AMPK-dependent Dmp53 activation in the FB in response to nutritional stress is required for proper communication between the FB and the IPCs by modulating the expression of *Drosophila* Leptin analog, Upd2. Elevated Upd2 levels and activation of JAK/STAT signaling in the brain of starved Dmp53-depleted animals result in sustained Dilp2 circulating levels, activation of insulin signaling and impaired autophagy induction in various tissues, therefore reducing survival rates upon nutrient deprivation. These results position AMPK-p53 axis as a key player in nutrient sensing and in regulating adaptive physiological responses to low nutrient availability by remotely controlling insulin secretion and autophagy.

Studies in mice have also shown that p53 is activated under several nutrient stress conditions such as nutrient deprivation, high-caloric and high-fat diets (HFD). P53 becomes activated under nutrient deprivation and regulates expression of genes involved in mitochondrial fatty acid uptake and oxidative phosphorylation (Liu et al., 2014). In turn, pharmacologic or genetic inhibition of p53 prevented excessive fat accumulation commonly observed under HFD (Derdak et al., 2013; Yokoyama et al., 2014) and resulted in decreased expression of proinflammatory cytokines and improved insulin resistance in mice with Type 2 Diabetes (T2D)-like disease (Minamino et al., 2009). Conversely, upregulation of p53 in adipose tissue caused an inflammatory response that led to insulin resistance

(Minamino et al., 2009). These results show that both mice and *Drosophila* p53 activation in individuals exposed to challenging nutrient conditions regulates global metabolism and directly contributes to diet associated-phenotypes.

P53-dependent Leptin regulation in animal physiology and disease

Leptin is mainly produced by adipose tissue in mice and humans, and regulates food intake, energy expenditure and metabolism acting mostly on neuronal targets in the brain. We have shown that Dmp53 activation in the FB under nutrient stress impacts systemic insulin signaling and autophagy induction via regulation of Upd2/Leptin expression. Notably, reduced survival of Dmp53 depleted animals to nutrient deprivation was highly reverted when inhibiting either Upd2 expression in the FB or JAK/STAT signaling in GABAergic neurons in the fly brain. Similar to Upd2, Leptin circulating levels decline during fasting conditions and are increased in animals fed with a HFD (Ahima et al., 1996; Frederich et al., 1995; Rajan and Perrimon, 2012; Rajan et al., 2017). Low Leptin levels during starvation trigger adaptive metabolic and hormonal responses, such as increased appetite and decreased energy expenditure (Ahima et al., 1996; Sano et al., 2015). In HFD fed mice, p53 activation is necessary for fat accumulation in the liver and adipose tissue indicating that p53 is essential for coordinating energy expenditure and storage in response to nutrient availability (Liu et al., 2017). Reduced expression of p53 target genes such as *GLUT4* and *SIRT1* has been proposed to reduce NAD+ levels and energy expenditure, leading to obesity (Liu et al., 2017). Alternatively, p53 activation in adipose cells could regulate Leptin expression which is known to act on the CNS to reduce food intake and enhance energy expenditure, thus limiting obesity in times of nutrient abundance. Further investigations into the role of adipose tissue p53 activity in modulating physiological and metabolic responses to stress will be necessary to have a better picture of the role p53 plays in the development of metabolic disorders such as obesity and T2D. Of importance, based on conserved adipose tissue-specific functions of p53 and signaling pathways involved, studies in *Drosophila* are likely to provide insights relevant to mammalian health and disease.

In the past decade, significant interest has been raised in understanding non-canonical functions of p53 that might have potential roles in tumor suppression (Ingaramo et al., 2018). The fact that p53 is activated in the adipose tissue of obese animals along with the results here presented concerning a putative direct role of p53 in controlling Upd2/Leptin expression demonstrate the importance of p53 in regulating metabolism. This is particularly interesting given that epidemiological studies over the last few decades have shown a strong influence of obesity on cancer risk and that increased Leptin can have hormone-like functions affecting tumor development (Andò et al., 2019; Maroni, 2020; Singh et al., 2020; Xu et al., 2019). In this context, our results give insights toward the molecular understanding of p53 activation under metabolic stress and its possible role in tumor suppression acting at either local or organismal level.

Regulation of adipose p53 function under metabolic stress

TOR and AMPK kinases play essential roles in nutrient sensing, are important regulators of energy balance at both cellular and whole-body levels, and have been shown to interact with p53 (Grewal, 2009; Hietakangas and Cohen, 2009; Jones et al., 2005). We previously

showed that TOR inhibition following long starvation treatments (24-48h) contributes to Dmp53 activation, mainly by alleviating miRNA-mediated targeting of Dmp53 in the FB (Barrio et al., 2014). In this work, we demonstrated that rapid activation of Dmp53 is dependent on AMPK and absolutely required for metabolic and physiological changes that promote organismal resistance to nutrient deprivation. This short-term activation of Dmp53 by AMPK could be part of a dual mechanism along with previously demonstrated long-term activation by lack of TOR, and both of these regulating mechanisms may be important for establishing a rapid response to transient acute nutrient stress also guaranteeing a sustained response when facing a much longer nutrient deprived period. Given that activated Dmp53 reduces Upd2 expression, systemic insulin and TOR signaling it would be reasonable to speculate that Dmp53-dependent TOR inhibition constitutes a positive feedback loop to reinforce Dmp53 activation upon long-term starvation conditions. Therefore, our results place p53 in a crucial position connecting nutrient sensing pathways to endocrine mechanisms, as part of a possible physiological feedback mechanism.

Drosophila AMPK activation has been shown to extend lifespan and promote tissue proteostasis through non-cell-autonomous regulation of autophagy (Stenesen et al., 2013; Ulgherait et al., 2014). Given that Dmp53, acting downstream of AMPK under nutrient stress, non-cell-autonomously regulates Dilp2 levels and autophagy it will be interesting to determine whether p53, and perhaps its direct phosphorylation by AMPK, is also required for extending organismal lifespan upon tissue-specific AMPK activation.

STAR METHODS

RESOURCE AVAILABILITY

Lead Contact—Further information and requests for resources and reagents should be directed to and will be fulfilled by the Lead Contact, Andrés Dekanty (adekanty@santafe-conicet.gov.ar).

Materials Availability—This study did not generate new unique reagents.

Data and Code Availability—Original images and data for figures are available upon request.

EXPERIMENTAL MODEL AND SUBJECT DETAILS

Drosophila melanogaster stocks were reared at 25°C on standard media containing: 4% glucose, 40 g/L powder yeast, 1% agar, 25 g/L wheat flour, 25 g/L cornflour, 4 ml/L propionic acid and 1.1 g/L nipagin. Fly stocks and their resources are listed in the Key Resources Table.

METHOD DETAILS

Fly husbandry and mosaic analysis—Gal4/UAS binary system was used to drive transgene expression in the different *Drosophila* tissues (Brand and Perrimon, 1993) and experimental crosses were performed at 25°C, unless otherwise specified. Crossing all Gal4 driver lines to w^{1118} background provided controls for each experiment. Flp/Out

system was used to generate GFP- or RFP-marked clones. Flies from Flp/Out lines (*hsFLP; act>y+>Gal4, UAS-RFP* or *hsFlp; UAS-Dicer2; R4-Cherry-atg8, act>y+>Gal4, UAS-GFP*) were crossed to corresponding UAS-transgene lines at 25°C and spontaneous recombination events taking place in the fat body prior to the onset of endoreplication were analyzed (Britton et al., 2002).

Starvation Treatments, High-Sugar Diet and Survival Experiments: For starvation treatments in larvae, eggs were collected for 4 h intervals and larvae were transferred to vials containing standard food immediately after eclosion (first instar larvae, L1) at a density of 50 larvae per tube. Larvae were then raised at 25°C for 72h prior to the starvation assay. Mid-third instar larvae were washed with PBS and placed in inverted 60 mm petri dishes with phosphate-buffered saline (PBS) soaked Whatman paper (starvation, STV) or maintained in standard food (well fed, WF). Each plate was sealed with parafilm and incubated at 25°C for the duration of the experiment. After the starvation period, full larvae or dissected fat bodies were used for immunostaining, RNA/protein extraction or metabolite measurements.

For starvation sensitivity assays, 5- to 7-day-old flies of each genotype were transferred into vials containing 2% agar in PBS. Flies were transferred to new tubes every day, and dead flies were counted every six hours. Control animals were always analyzed in parallel in each experimental condition. Statistics were performed using GraphPad Prism 6.0 software, which uses the Kaplan-Meier estimator to calculate survival fractions as well as median and maximum survival values. Curves were compared using the log-rank (Mantel-Cox) test. The two-tailed p value indicates the value of the difference between the two entire survival distributions at comparison. For chloroquine and rapamycin treatments, adults were transferred to food containing 2.5 mg/ml of chloroquine (Sigma), 400 uM of rapamycin (LC Labs) or an equivalent volume of ethanol as a control. Number of individuals used in each experiment is detailed in Table S1.

For high-sugar diet (HSD) experiments, eggs were collected for 4h interval and larvae were transferred to either standard (4% sucrose) or high-sugar (34% sucrose) food immediately after eclosion (50 L1 larvae per tube). Mid-third instar larvae were used for immunoassay (Dilp2 circulating levels), and 5- to 7-day-old flies were used for RNA extraction. Survival rates were measured as the percent of individuals entering pupariation. At least 120 larvae per genotype were scored. Data were normalized with respect to the control genotype and Student’s t-test analysis was carried out for statistical significance.

Immunostainings: Mid-third instar larvae were dissected in cold PBS and fixed in 4% formaldehyde/PBS for 20 min at room temperature. Inverted larvae and dissected tissues from ex vivo experiments were directly fixed after incubation. They were then washed and permeabilized in PBT (0.2% Triton X-100 in PBS) for 30 min and blocked in BBT (0.3% BSA, 250 mM NaCl in PBT) for 1 h. Samples were incubated overnight at 4°C with primary antibody diluted in BBT, washed three times (15 min each) in BBT and incubated with secondary antibodies for 1.5 hour at room temperature. After three washes with PBT (15 min each), dissected tissues were placed in mounting medium (80% glycerol/PBS containing 0.05% n-Propyl-Gallate). Images were acquired on a Leica SP8 inverted confocal

microscope and analyzed and processed using Fiji (Schindelin et al., 2012) and Adobe Photoshop. The following primary antibodies were used: rabbit anti-β-Gal (A11132, Invitrogen); rat anti-Dilp2 (Géminard et al., 2009), mouse anti-GFP (12A6, DSHB). The following secondary antibodies were used: anti-mouse IgG-Alexa Fluor 594; anti-mouse IgG-Alexa Fluor 488; anti-rabbit IgG-Alexa Fluor 594; and anti-rabbit IgG-Alexa Fluor 488 (Jackson InmunoResearch). Antibodies and their resources are listed in the Key Resources Table.

For Lysotracker staining, five mid-third instar larvae either well fed or starved were dissected in cold PBS and incubated 5 min with LysoTracker Green (ThermoFisher) at a final concentration of 0,5 μM in PBS. After washing, dissected tissues were placed in mounting medium (80% glycerol/PBS containing 0.05% n-Propyl-Gallate) and immediately imaged.

Western blot: Dissected fat bodies were homogenized and lysed in 25 μl of cell lysis buffer (Cell Signalling), supplemented with protease inhibitor cocktail (Halt Protease Inhibitor Cocktail, Thermo Fisher Scientific) and protein concentration was determined (Bio-Rad Protein Assay). Twenty-five micrograms of protein extracts were loaded and separated in 4-20% SDS polyacrylamide gel electrophoresis (Mini-PROTEAN® TGX™ Precast Protein Gels) and blotted onto PVDF membranes (Immobilion-P, Millipore). Membranes were blocked for 1 hour at room temperature with 5% BSA in TBS-T (TBS with 0.1% Tween 20) and then incubated overnight with mouse anti-actin (DSHB) and rabbit anti-phospho-Drosophila S6 Kinase (Cell Signaling) antibodies in TBS-T. Membranes were extensively washed and incubated for 1 hour at room temperature with a peroxidase-conjugated anti-mouse or anti-rabbit secondary antibody (ThermoFisher). Immunoblots were developed with SuperSignal™ West Pico PLUS Chemiluminescent Substrate (ThermoFisher), imaged with ChemiDoc imager (Bio-Rad) and quantitated using Fiji. Phospho-S6K levels were normalized to actin and represented as fold change respect to control, well fed animals. Data represent mean± SEM of three independent experiments.

RNA isolation and quantitative RT-PCR: To measure mRNA levels, total RNA was extracted from adults, whole larvae, or dissected FBs of 30 animals using TRIZOL RNA Isolation Reagent (Invitrogen). First strand cDNA synthesis was performed using an oligo(dT)18 primer and RevertAid reverse transcriptase (ThermoFisher) under standard conditions. Quantitative PCR was performed on an aliquot of the cDNA with specific primers using the StepOnePlus Real-Time PCR System. Expression values were normalized to *actin* transcript levels. Data were then normalized to control WF animals using the ΔΔ-CT and fold change was calculated afterwards. In all cases, three independent samples were collected from each condition and genotype. Student's t test was used for statistical analysis.

Circulating Dilp2 levels in hemolymph: Dilp2 circulating levels in the hemolymph of well-fed or starved animals were quantified by sandwich ELISA as previously described (Park et al., 2014). Hemolymph was obtained by bleeding washed larvae on ice, and collected in tubes with 55 μL cold PBS. Supernatant after centrifugation at 1,000 x g for one minute was used for ELISA. Briefly, coated plates (Greiner 655061) were incubated overnight at 4°C with monoclonal anti-FLAG antibody (2.5 μg/ml, Sigma F1804) diluted

in 0.2M sodium carbonate/bicarbonate buffer, pH 9.4. Plates were washed with PBTw (0,2% Tween-20 in PBS) and blocked with PBS containing 2% BSA overnight at 4°C. Plates were then washed with PBTw before adding hemolymph. Samples were mixed with anti-HA-Peroxidase (Roche #12013819001) at a dilution of 1:350 in PBS-Tween-20 2%, added to plates and incubated overnight at 4°C. Plates were extensively washed with PBTw and incubated with 1-Step Ultra TMB-ELISA Substrate (ThermoFisher #34029) for 25 min at RT. The reaction was stopped by adding 2M sulfuric acid and absorbance was measured immediately at 450nm.

Fluorescence quantification in IPCs and FB cells: For fluorescence quantification, confocal Z series were taken using a Leica SP8 confocal microscope as described below and identical microscope settings and all subsequent treatments of images were used for control and experimental samples. Total fluorescence intensity of maximum Z-projections was measured using Fiji and data were normalized to control animals. Student's t-test analysis was carried out for statistical significance. To quantify Dilp2 intensity levels in larval brains, confocal sections covering the entire IPCs were obtained. To quantify β-gal (*unk-lacZ* reporter) intensity levels in FB cells, confocal sections covering the entire nuclei were taken from 10 FBs and nuclei fluorescence were assessed. To quantify membrane GFP (tGPH reporter) intensity levels, confocal sections covering a 5 micron plasma membrane section were taken from 10 FBs. To quantify Lysotracker intensity levels and mCherry-ATG8 positive punctae, randomly selected pictures were loaded in FIJI and automatically processed. Total fluorescence intensity (Lysotracker) and area (mCh-ATG8) were scored and normalized to control animals. At least 10 images taken from 6-8 animals, and 2-3 independent experiments, per genotype and condition were analyzed. Student's t test was used for statistical analysis.

Ex vivo experiments: For *ex vivo* incubation experiments of whole inverted larvae (carcasses containing fat body, brain and other tissues) sixteen mid-third instar larvae per condition were used. After washing and disection, inverted larvae were incubated in 50 μL of Shields and Sang M3 Insect Medium (Sigma) at room temperature for 3 h. Incubation of inverted larvae in M3 medium has been previously shown to reduce TOR pathway activity and induce autophagy resembling starvation (Kim and Neufeld, 2015). Inverted animals were then fixed, permeabilized, and inmunostained as described above using rat anti-Dilp2 antibodies (1/400). In the case of co-culture experiments, eight inverted larvae from each genotype (cg>GFP and cg>$p53^{H159.N}$) were incubated together in M3 medium and all subsequent steps were performed in the same tube to minimize variability. Dissected brains from 6-8 larvae per genotype and condition were imaged and used for quantification.

For *ex vivo* incubation experiments of dissected tissues, brains from eight wild type mid-third instar larvae were co-incubated with eight dissected fat bodies from the different genotypes (cg>GFP and cg>$p53^{H159.N}$) in 25 μL of M3 medium at room temperature for 3 h. After immunostaining with anti-Dilp2 antibodies, five brains were placed in mounting medium, imaged, and Dilp2 fluorescence quantified.

Metabolic Assays: TAG, glycogen and glucose levels were determined as previously described (Barrio et al., 2014). Briefly, mid-third instar larvae or 5-7 days old adult flies

were fast frozen in liquid nitrogen, homogenized in 200 μl of PBS and immediately incubated at 70°C for 10 min to inactivate endogenous enzymes. For quantification of glucose, hemolymph from 15 larvae was diluted 1:100 and incubated at 70°C for 5 min. TAG levels were determine using a serum triglyceride determination kit (Sigma, TR0100) according to the manufacturer's protocol. For glycogen measurements, 40 μl of heat-treated homogenates were incubated with or without 1 unit of Amyloglucosidase (Sigma, A7420) for 2 hr at 55°C and assayed using a Glucose (GO) Assay Kit (Sigma, GAGO-20). Glycogen amounts were determined by subtracting from the total amount of glucose present in the sample treated with amiloglucosidase the amount of free glucose of untreated samples. Metabolite levels were normalized to protein concentration (BioRad Protein Assay). Five replicates for each genotype and condition were performed, and data were represented as a percentage of the corresponding levels in fed condition for each genotype.

Developmental timing and pupal size: For developmental timing, eggs were collected for 4h interval and first instar larvae were transferred to new vials containing either standard (4% sucrose) or high-sugar (34% sucrose) food immediately after eclosion at a density of 50 larvae per tube. Larvae were then raised at 25°C and the number of pupae was counted at different time points. Five replicates for each genotype and condition were performed, and the resulting percentage of pupae was calculated.

For pupal size measurements, volume was calculated by the formula $4/3\pi(L/2)(l/2)2$ (L, length; l, diameter). Images were taken with a Leica MZ10F Stereoscope, and measures were done using ImageJ software. Pupal size values were shown as the ratio with respect to control animals.

QUANTIFICATION AND STATISTICAL ANALYSIS

For starvation sensitivity assays statistics were performed using GraphPad Prism6, which uses the Kaplan-Meier estimator to calculate survival fractions as well as median and maximum survival values. Curves were compared using the log-rank (Mantel-Cox) test. The two-tailed p value indicates the value of the difference between the two entire survival distributions at comparison.

Graphpad Prism6 was used for statistical analysis and graphical representations based on three or more replicates for each experiment. All significance tests were carried out with unpaired two tailed Student's t tests. Significance P values: *$p < 0.05$, **$p < 0.01$, ***$p < 0.001$, ****$p < 0.0001$, $^{ns}p > 0.05$.

Images were acquired on a Leica SP8 inverted confocal microscope and analyzed and processed using Fiji (Schindelin et al., 2012) and Adobe Photoshop. Tissue orientation and/or position was adjusted in the field of view for images presented. No relevant information was affected. The original images are available upon request.

Supplementary Material

Refer to Web version on PubMed Central for supplementary material.

Acknowledgements

We thank Daniel Gonzalez and Pablo Wappner for support and reagents, Pierre Leopold, Aurelio Teleman, Vienna *Drosophila* RNAi Center, *Drosophila* Bloomington Stock Center, and the Developmental Studies Hybridoma Bank for flies and antibodies. We also thank Rich Binari for help with managing fly stocks, Pablo Manavella, Ilia Droujinine, Ying Liu, Nirmalya Chatterjee for comments on the manuscript.

M.C.I and J.A.S are funded by PhD fellowships from CONICET. N.P is an Investigator of the Howard Hughes Medical Institute. A.D. is a member of CONICET and Professor at UNL. This work was supported by grants from the Agencia Nacional de Promoción Cientifica y Tecnológica, Argentina (ANPCyT), Universidad Nacional del Litoral (UNL) and MinCyT-DAAD Bilateral Cooperation Program.

REFERENCES

Agrawal N, Delanoue R, Mauri A, Basco D, Pasco M, Thorens B, and Léopold P (2016). The Drosophila TNF Eiger Is an Adipokine that Acts on Insulin-Producing Cells to Mediate Nutrient Response. Cell Metab. 23, 675–684. [PubMed: 27076079]

Ahima RS, Prabakaran D, Mantzoros C, Qu D, Lowell B, Maratos-Flier E, and Flier JS (1996). Role of leptin in the neuroendocrine response to fasting. Nature 382, 250–252. [PubMed: 8717038]

Andersen DS, Colombani J, and Léopold P (2013). Coordination of organ growth: principles and outstanding questions from the world of insects. Trends Cell Biol. 23, 336–344. [PubMed: 23587490]

Andò S, Gelsomino L, Panza S, Giordano C, Bonofiglio D, Barone I, and Catalano S (2019). Obesity, Leptin and Breast Cancer: Epidemiological Evidence and Proposed Mechanisms. Cancers (Basel). 11.

Arrese EL, and Soulages JL (2010). Insect fat body: energy, metabolism, and regulation. Annu. Rev. Entomol 55, 207–225. [PubMed: 19725772]

Arsham AM, and Neufeld TP (2009). A genetic screen in Drosophila reveals novel cytoprotective functions of the autophagy-lysosome pathway. PLoS One 4.

Barrio L, Dekanty A, and Milán M (2014). MicroRNA-Mediated Regulation of Dp53 in the Drosophila Fat Body Contributes to Metabolic Adaptation to Nutrient Deprivation. Cell Rep. 8, 528–541. [PubMed: 25017064]

Bauer JH, Chang C, Morris SNS, Hozier S, Andersen S, Waitzman JS, and Helfand SL (2007). Expression of dominant-negative Dmp53 in the adult fly brain inhibits insulin signaling. Proc. Natl. Acad. Sci. U. S. A 104, 13355–13360. [PubMed: 17686972]

Berkers CR, Maddocks ODK, Cheung EC, Mor I, and Vousden KH (2013). Metabolic Regulation by p53 Family Members. Cell Metab. 18, 617–633. [PubMed: 23954639]

Brand a H., and Perrimon N (1993). Targeted gene expression as a means of altering cell fates and generating dominant phenotypes. Development 118, 401–415. [PubMed: 8223268]

Britton JS, and Edgar BA (1998). Environmental control of the cell cycle in Drosophila : nutrition activates mitotic and endoreplicative cells by distinct mechanisms. 2158, 2149–2158.

Britton JS, Lockwood WK, Li L, Cohen SM, and Edgar BA (2002). Drosophila ' s Insulin/PI3-Kinase Pathway Coordinates Cellular Metabolism with Nutritional Conditions. 2, 239–249.

Contreras EG, Sierralta J, and Glavic A (2018). P53 is required for brain growth but is dispensable for resistance to nutrient restriction during Drosophila larval development. PLoS One 13, 1–17.

Delanoue R, Meschi E, Agrawal N, Mauri A, Tsatskis Y, McNeill H, and Léopold P (2016). Drosophila insulin release is triggered by adipose Stunted ligand to brain Methuselah receptor. Science (80-.). 353, 1553–1556.

Derdak Z, Villegas KA, Harb R, Wu AM, Sousa A, and Wands JR (2013). Inhibition of p53 attenuates steatosis and liver injury in a mouse model of non-alcoholic fatty liver disease. J. Hepatol 58, 785–791. [PubMed: 23211317]

Frederich RC, Hamann A, Anderson S, Löllmann B, Lowell BB, and Flier JS (1995). Leptin levels reflect body lipid content in mice: evidence for diet-induced resistance to leptin action. Nat. Med 1, 1311–1314. [PubMed: 7489415]

Géminard C, Rulifson EJ, and Léopold P (2009). Remote Control of Insulin Secretion by Fat Cells in Drosophila. Cell Metab. 10, 199–207. [PubMed: 19723496]

Grewal SS (2009). Insulin/TOR signaling in growth and homeostasis: a view from the fly world. Int. J. Biochem. Cell Biol 41, 1006–1010. [PubMed: 18992839]

Hasygar K, and Hietakangas V (2014). p53- and ERK7-Dependent Ribosome Surveillance Response Regulates Drosophila Insulin-Like Peptide Secretion. PLoS Genet. 10, e1004764. [PubMed: 25393288]

Hietakangas V, and Cohen SM (2009). Regulation of tissue growth through nutrient sensing. Annu. Rev. Genet 43, 389–410. [PubMed: 19694515]

Ikeya T, Galic M, Belawat P, Nairz K, and Hafen E (2002). Nutrient-dependent expression of insulin-like peptides from neuroendocrine cells in the CNS contributes to growth regulation in Drosophila. Curr. Biol 12, 1293–1300. [PubMed: 12176357]

Ingaramo MC, Sánchez JA, and Dekanty A (2018). Regulation and function of p53: A perspective from Drosophila studies. Mech. Dev 154, 82–90. [PubMed: 29800619]

Jiang P, Du W, Wang X, Mancuso A, Gao X, Wu M, and Yang X (2011). p53 regulates biosynthesis through direct inactivation of glucose-6-phosphate dehydrogenase. Nat. Cell Biol 13, 310–316. [PubMed: 21336310]

Johnson EC, Kazgan N, Bretz CA, Forsberg LJ, Hector CE, Worthen RJ, Onyenwoke R, and Brenman JE (2010). Altered metabolism and persistent starvation behaviors caused by reduced AMPK function in Drosophila. PLoS One 5.

Jones RG, Plas DR, Kubek S, Buzzai M, Mu J, Xu Y, Birnbaum MJ, and Thompson CB (2005). AMP-activated protein kinase induces a p53-dependent metabolic checkpoint. Mol. Cell 18, 283–293. [PubMed: 15866171]

Kim J, and Neufeld TP (2015). Dietary sugar promotes systemic TOR activation in Drosophila through AKH-dependent selective secretion of Dilp3. Nat. Commun 6, 6846. [PubMed: 25882208]

Koyama T, and Mirth CK (2016). Growth-Blocking Peptides As Nutrition-Sensitive Signals for Insulin Secretion and Body Size Regulation. PLoS Biol. 14, 1–23.

Kudron MM, Victorsen A, Gevirtzman L, Hillier LW, Fisher WW, Vafeados D, Kirkey M, Hammonds AS, Gersch J, Ammouri H, et al. (2018). The ModERN Resource: Genome-Wide Binding Profiles for Hundreds of Drosophila and Caenorhabditis elegans Transcription Factors. Genetics 208, 937–949. [PubMed: 29284660]

Kurtz P, Jones AE, Tiwari B, Link N, Wylie A, Tracy C, Krámer H, and Abrams JM (2019). *Drosophila* p53 directs non-apoptotic programs in postmitotic tissue. Mol. Biol. Cell mbcE18-12-0791.

De La Cova C, Senoo-Matsuda N, Ziosi M, Wu DC, Bellosta P, Quinzii CM, and Johnston LA (2014). Supercompetitor status of drosophila Myc cells requires p53 as a Fitness sensor to reprogram metabolism and promote viability. Cell Metab. 19, 470–483. [PubMed: 24561262]

Liang Y, Liu J, and Feng Z (2013). The regulation of cellular metabolism by tumor suppressor p53. Cell Biosci. 3, 9. [PubMed: 23388203]

Liu S, Kim TH, Franklin DA, and Zhang Y (2017). Protection against High-Fat-Diet-Induced Obesity in MDM2C305F Mice Due to Reduced p53 Activity and Enhanced Energy Expenditure. Cell Rep. 18, 1005–1018. [PubMed: 28122227]

Liu Y, He Y, Jin A, Tikunov AP, Zhou L, Tollini LA, Leslie P, Kim T-H, Li LO, Coleman RA, et al. (2014). Ribosomal protein-Mdm2-p53 pathway coordinates nutrient stress with lipid metabolism by regulating MCD and promoting fatty acid oxidation. Proc. Natl. Acad. Sci 111, E2414–E2422. [PubMed: 24872453]

Lu W-J, Chapo J, Roig I, and Abrams JM (2010). Meiotic Recombination Provokes Functional Activation of the p53 Regulatory Network. Science (80-.). 328, 1278–1281.

Maddocks ODK, Berkers CR, Mason SM, Zheng L, Blyth K, Gottlieb E, and Vousden KH (2013). Serine starvation induces stress and p53-dependent metabolic remodelling in cancer cells. Nature 493, 542–546. [PubMed: 23242140]

Mandal S, Freije W. a, Guptan P, and Banerjee U (2010). Metabolic control of G1-S transition: cyclin E degradation by p53-induced activation of the ubiquitin-proteasome system. J. Cell Biol 188, 473–479. [PubMed: 20176921]

Maroni P (2020). Leptin, Adiponectin, and Sam68 in Bone Metastasis from Breast Cancer. Int. J. Mol. Sci 21, 1051.

Meschi E, Léopold P, and Delanoue R (2019). An EGF-Responsive Neural Circuit Couples Insulin Secretion with Nutrition in Drosophila. Dev. Cell 48, 76–86.e5. [PubMed: 30555002]

Mesquita D, Dekanty A, and Milán M (2010). A dp53-dependent mechanism involved in coordinating tissue growth in Drosophila. PLoS Biol. 8.

Minamino T, Orimo M, Shimizu I, Kunieda T, Yokoyama M, Ito T, Nojima A, Nabetani A, Oike Y, Matsubara H, et al. (2009). A crucial role for adipose tissue p53 in the regulation of insulin resistance. Nat. Med 15, 1082–1087. [PubMed: 19718037]

Musselman LP, and Kühnlein RP (2018). Drosophila as a model to study obesity and metabolic disease. J. Exp. Biol 121.

Park S, Alfa RW, Topper SM, Kim GES, Kockel L, and Kim SK (2014). A Genetic Strategy to Measure Circulating Drosophila Insulin Reveals Genes Regulating Insulin Production and Secretion. PLoS Genet. 10, e1004555. [PubMed: 25101872]

Puig O, Marr MT, Ruhf ML, and Tjian R (2003). Control of cell number by Drosophila FOXO: downstream and feedback regulation of the insulin receptor pathway. Genes Dev. 17, 2006–2020. [PubMed: 12893776]

Rajan A, and Perrimon N (2012). Drosophila cytokine unpaired 2 regulates physiological homeostasis by remotely controlling insulin secretion. Cell 151, 123–137. [PubMed: 23021220]

Rajan A, Housden BE, Wirtz-Peitz F, Holderbaum L, and Perrimon N (2017). A Mechanism Coupling Systemic Energy Sensing to Adipokine Secretion. Dev. Cell 43, 83–98.e6. [PubMed: 29017032]

Robin M, Issa AR, Santos CC, Napoletano F, Petitgas C, Chatelain G, Ruby M, Walter L, Birman S, Domingos PM, et al. (2019). Drosophila p53 integrates the antagonism between autophagy and apoptosis in response to stress. Autophagy 15, 771–784. [PubMed: 30563404]

Rulifson EJ, Kim SK, and Nusse R (2002). Ablation of insulin-producing neurons in flies: growth and diabetic phenotypes. Science 296, 1118–1120. [PubMed: 12004130]

Rusten TE, Lindmo K, Juhász G, Sass M, Seglen PO, Brech A, and Stenmark H (2004). Programmed autophagy in the Drosophila fat body is induced by ecdysone through regulation of the PI3K pathway. Dev. Cell 7, 179–192. [PubMed: 15296715]

Sanchez JA, Mesquita D, Ingaramo MC, Ariel F, Milán M, and Dekanty A (2019). Eiger/TNFα-mediated Dilp8 and ROS production coordinate intra-organ growth in Drosophila. PLOS Genet. 15, e1008133. [PubMed: 31425511]

Sano H, Nakamura A, Texada MJ, Truman JW, Ishimoto H, Kamikouchi A, Nibu Y, Kume K, Ida T, and Kojima M (2015). The Nutrient-Responsive Hormone CCHamide-2 Controls Growth by Regulating Insulin-like Peptides in the Brain of Drosophila melanogaster. PLOS Genet. 11, e1005209. [PubMed: 26020940]

Scherz-Shouval R, Weidberg H, Gonen C, Wilder S, Elazar Z, and Oren M (2010). p53-dependent regulation of autophagy protein LC3 supports cancer cell survival under prolonged starvation. Proc. Natl. Acad. Sci. U. S. A 107, 18511–18516. [PubMed: 20937856]

Schindelin J, Arganda-Carreras I, Frise E, Kaynig V, Longair M, Pietzsch T, Preibisch S, Rueden C, Saalfeld S, Schmid B, et al. (2012). Fiji: an open-source platform for biological-image analysis. Nat. Methods 9, 676–682. [PubMed: 22743772]

Scott RC, Schuldiner O, and Neufeld TP (2004). Role and regulation of starvation-induced autophagy in the Drosophila fat body. Dev. Cell 7, 167–178. [PubMed: 15296714]

Singh S, Mayengbam SS, Chouhan S, Deshmukh B, Ramteke P, Athavale D, and Bhat MK (2020). Role of TNFα and leptin signaling in colon cancer incidence and tumor growth under obese phenotype. Biochim. Biophys. Acta - Mol. Basis Dis 1866, 165660. [PubMed: 31891805]

Stenesen D, Suh JM, Seo J, Yu K, Lee J-S, Kim J-S, Min K-J, and Graff JM (2013). Adenosine nucleotide biosynthesis and AMPK regulate adult life span and mediate the longevity benefit of caloric restriction in flies. Cell Metab. 17, 101–112. [PubMed: 23312286]

Taguchi A, and White MF (2008). Insulin-like signaling, nutrient homeostasis, and life span. Annu. Rev. Physiol 70, 191–212. [PubMed: 17988211]

Tajan M, Hock AK, Blagih J, Robertson NA, Labuschagne CF, Kruiswijk F, Humpton TJ, Adams PD, and Vousden KH (2018). A Role for p53 in the Adaptation to Glutamine Starvation through the Expression of SLC1A3. Cell Metab. 28, 721–736.e6. [PubMed: 30122553]

Teleman AA, Chen Y, and Cohen SM (2005). 4E-BP functions as a metabolic brake used under stress conditions but not during normal growth. 1844–1848. [PubMed: 16103212]

Tiebe M, Lutz M, De La Garza A, Buechling T, Boutros M, and Teleman AA (2015). REPTOR and REPTOR-BP Regulate Organismal Metabolism and Transcription Downstream of TORC1. Dev. Cell 33, 272–284. [PubMed: 25920570]

Ulgherait M, Rana A, Rera M, Graniel J, and Walker DW (2014). AMPK modulates tissue and organismal aging in a non-cell-autonomous manner. Cell Rep. 8, 1767–1780. [PubMed: 25199830]

Wu Q, and Brown MR (2006). Signaling and function of insulin-like peptides in insects. Annu. Rev. Entomol 51, 1–24. [PubMed: 16332201]

Xu Y, Tan M, Tian X, Zhang J, Zhang J, Chen J, Xu W, and Sheng H (2019). Leptin receptor mediates the proliferation and glucose metabolism of pancreatic cancer cells via AKT pathway activation. Mol. Med. Rep 21, 945–952. [PubMed: 31789415]

Yokoyama M, Okada S, Nakagomi A, Moriya J, Shimizu I, Nojima A, Yoshida Y, Ichimiya H, Kamimura N, Kobayashi Y, et al. (2014). Inhibition of endothelial p53 improves metabolic abnormalities related to dietary obesity. Cell Rep. 7, 1691–1703. [PubMed: 24857662]

Yu-Yun Chang, and Neufeld Thomas P. (2009). An Atg1/Atg13 Complex with Multiple Roles in TOR-mediated Autophagy Regulation. Mol. Biol. Cell 20, 2004–2014. [PubMed: 19225150]

Zawacka-Pankau J, Grinkevich VV, Hünten S, Nikulenkov F, Gluch A, Li H, Enge M, Kel A, and Selivanova G (2011). Inhibition of Glycolytic Enzymes Mediated by Pharmacologically Activated p53. J. Biol. Chem 286, 41600–41615. [PubMed: 21862591]

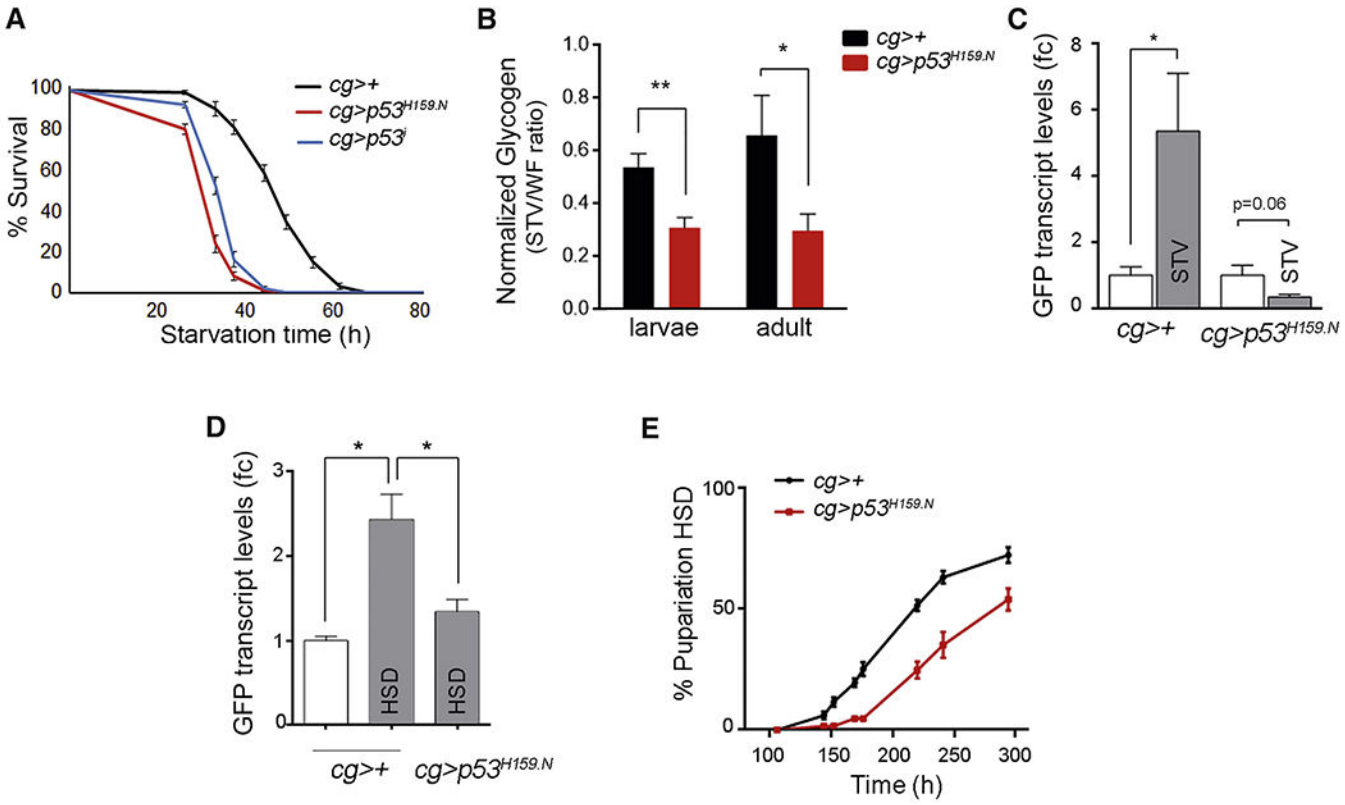

Fig. 1: Fat body Dmp53 regulates organismal response to challenging nutrient conditions

(A) Reduced survival rates to nutrient deprivation of adult flies (males) expressing *Dmp53*$^{H159.N}$ (*cg>p53*$^{H159.N}$) or *Dmp53*^{RNAi}(*cg>p53*)^{i} under *cg*-Gal4 control. See Table S1 for n, p, median, and maximum survival values. (B)Glycogen content in whole larvae and adult flies from the indicated genotypes subjected to starvation (4h in larvae; 24h in adults). Data were normalized to protein concentration and presented as a ratio STV/WF for each genotype. (C-D) qRT-PCR showing *GFP* mRNA levels in whole larvae (C) and adult flies (D) bearing p53^{RE}-GFP activity reporter and expressing the indicated transgenes under well fed (WF), starved (STV) or high-sugar diet (HSD) conditions. Results are expressed as fold induction respect to control WF animals. Three independent replicates were carried out for each sample. (E) Development timing of control (*cg*)>+) and *cg>p53*$^{H159.N}$ animals raised immediately after hatching in HSD.

Mean ± SEM. * p<0.05; ** p<0.01.

See also Figure S1 and Table S1.

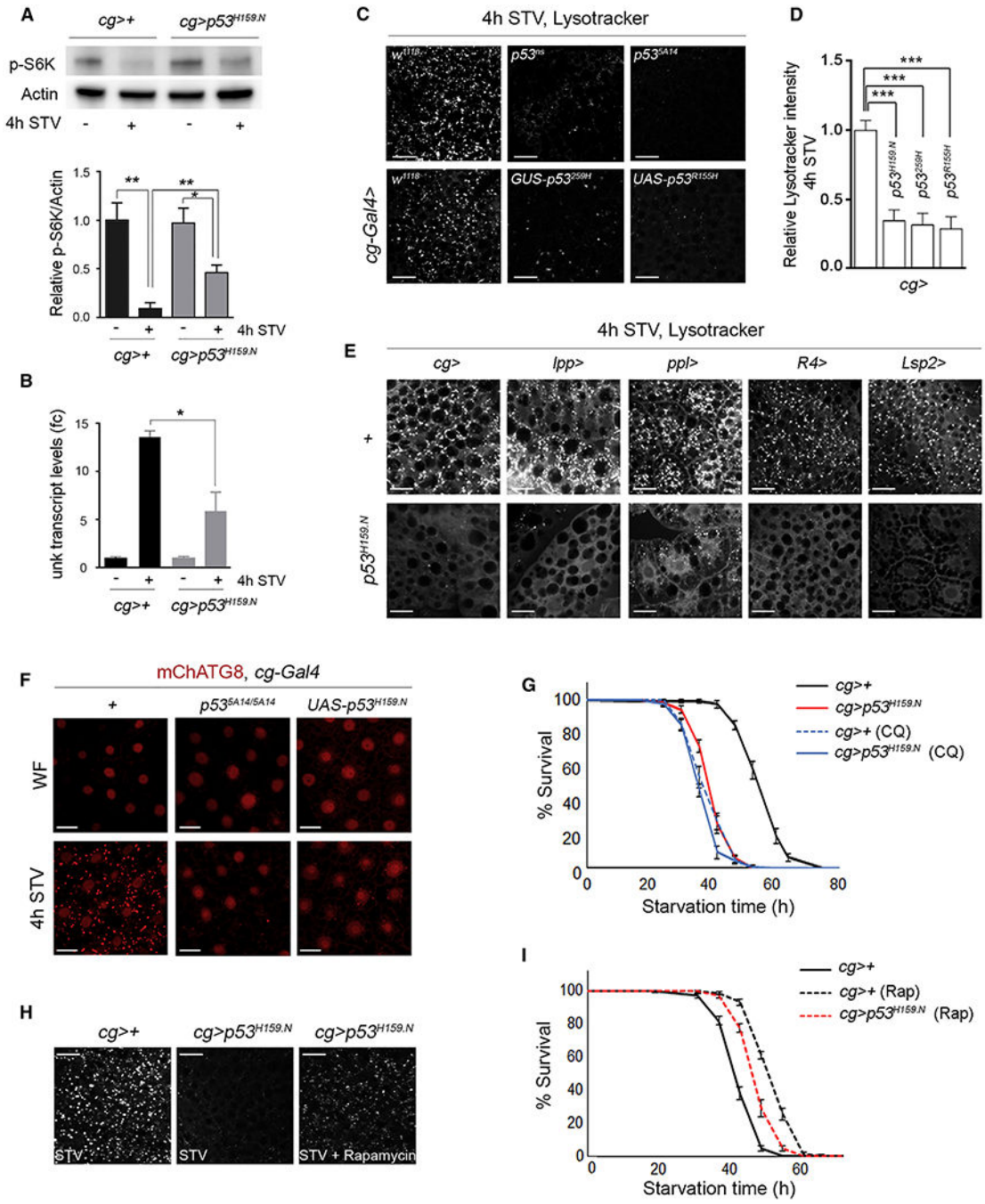

Fig. 2: Fat body Dmp53 regulates TOR signaling, autophagy induction and survival upon starvation

(A) Inmunoblot showing p-S6K levels in FB extracts from control (*cg*>+) and *cg>p53*$^{H159.N}$ animals in WF and STV conditions. Data were normalized to actin levels and expressed relative to WF animals. Mean ±SEM of 3 independent experiments are shown. (B) qRT-PCR showing *unk* transcript levels in FB samples obtained from *cg*>+ and *cg>p53*$^{H159.N}$ larvae in WF or STV conditions. Results are expressed as fold induction respect to control animals. Three independent replicates were carried out for each sample. (C) Lysotracker staining to detect autophagy induction in the FB of starved control (*w*^{1118} or *cg>+), dmp53* mutant

(*p53*^{ns} or *p53*^{5A14}) and Dmp53-depleted (*cg>p53*^{259H} or *cg>p53*^{R155H}) larvae. (D) Relative lysotracker intensity of the indicated genotypes. n≥ 10 for 2 independent experiments. (E) Lysotracker staining of starved larvae expressing *Dmp53*$^{H159.N}$ in the FB under the control of the indicated Gal4 drivers. In all the cases, expression of *Dmp53*$^{H159.N}$ strongly reduced starvation-induced autophagy. (F) FB cells labelled to visualize autophagic vesicles by using mCherry-Atg8 fusion protein (mChAtg8; in red) in control, p53$^{5A14/5A14}$ and *cg>p53*$^{H159.N}$ animals in WF or STV conditions. (G and I) Survival rates to nutrient deprivation of adult flies (males) expressing the indicated transgenes under *cg*-Gal4 control and treated with Chloroquine (G), Rapamycin (I) or the corresponding vehicles. See Table S1 for n, p, median, and maximum survival values. (H) Lysotracker staining showing that reduced autophagy induction observed in starved *cg>p53*$^{H159.N}$ larvae was partially rescued by Rapamycin treatment.

Mean ± SEM. ***p<0.001; **p<0.01; *p<0.05. Scale bars, 25 μm.

See also Figure S2 and Table S1.

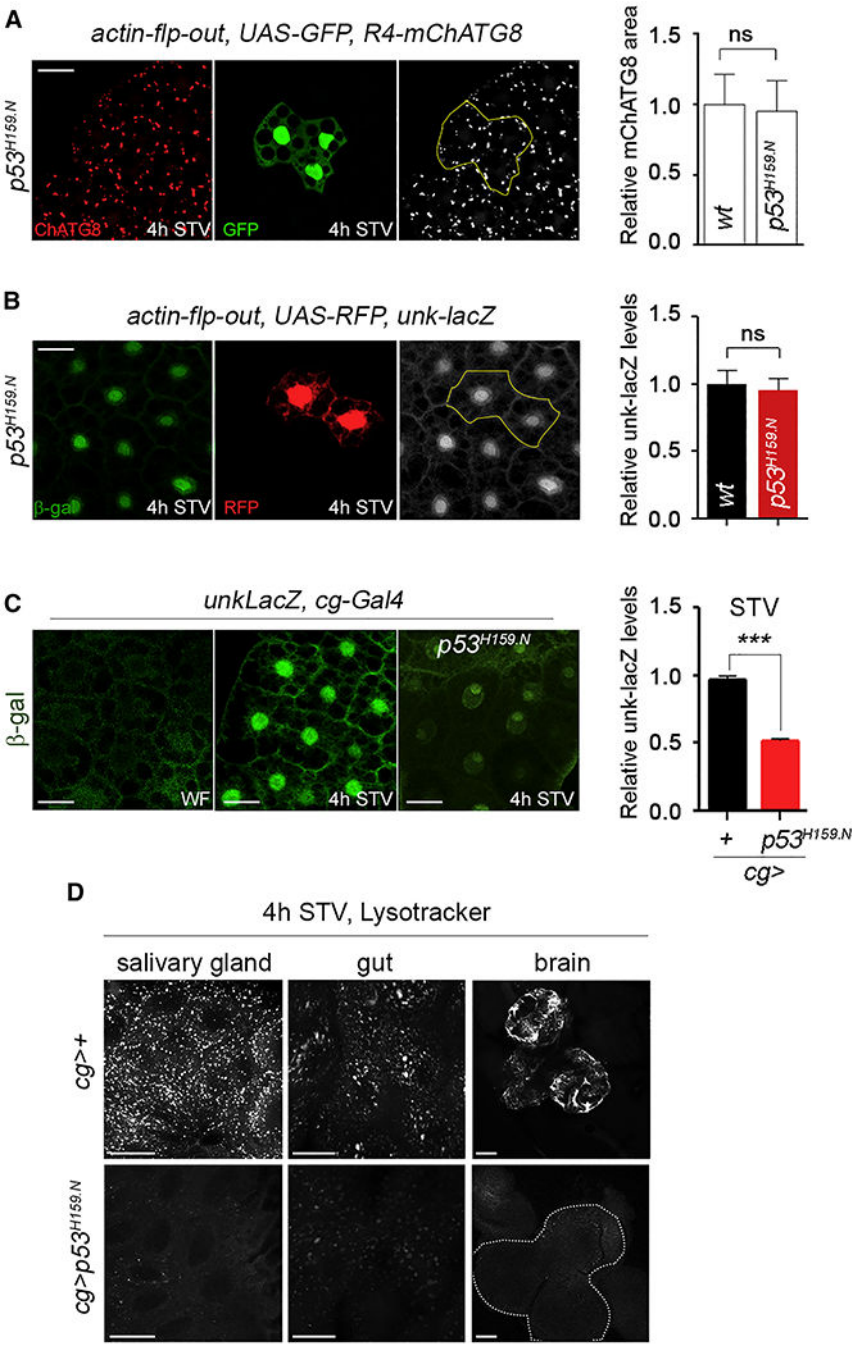

Fig. 3: Dmp53 non-cell-autonomously regulates TOR signaling and autophagy upon starvation

(A) FB cells labelled to visualize mCherry-Atg8 fusion protein (mChAtg8; in red or white). Starved FB cells expressing *Dmp53*$^{H159.N}$ (marked by the expression of GFP, in green) showed similar autophagy induction than neighboring wild-type cells (left). Relative mChAtg8 area (right) between control and *Dmp53*$^{H159.N}$ expressing cells are shown. n≥ 10 for 3 independent experiments. (B) Immunostaining showing *unk-lacZ* expression (β-gal in green or white). Starved FB cells expressing *Dmp53*$^{H159.N}$ (marked by the expression of RFP, in red) showed similar *unk-lacZ* levels than neighboring wild-type cells. Relative

unk-lacZ levels between control and *Dmp53*$^{H159.N}$ expressing cells are shown (right). n≥ 10 for 3 independent experiments. (C) Immunostaining showing *unk-lacZ* levels (β-gal, green) in the FB of *cg>+* and *cg>p53*$^{H159.N}$ larvae in WF or STV conditions. Relative β-gal fluorescence intensity showing sustained *unk-lacZ* levels in starved *cg>p53*$^{H159.N}$ animals (right). n≥ 50 for 3 independent experiments. (D) Lysotracker staining to detect autophagy induction in the salivary gland, intestine and brain of starved *cg>+* and *cg>p53*$^{H159.N}$ larvae. Mean ± SEM. ***p<0.001; ns: not significant. Scale bars, 30 μm.
See also Figure S3.

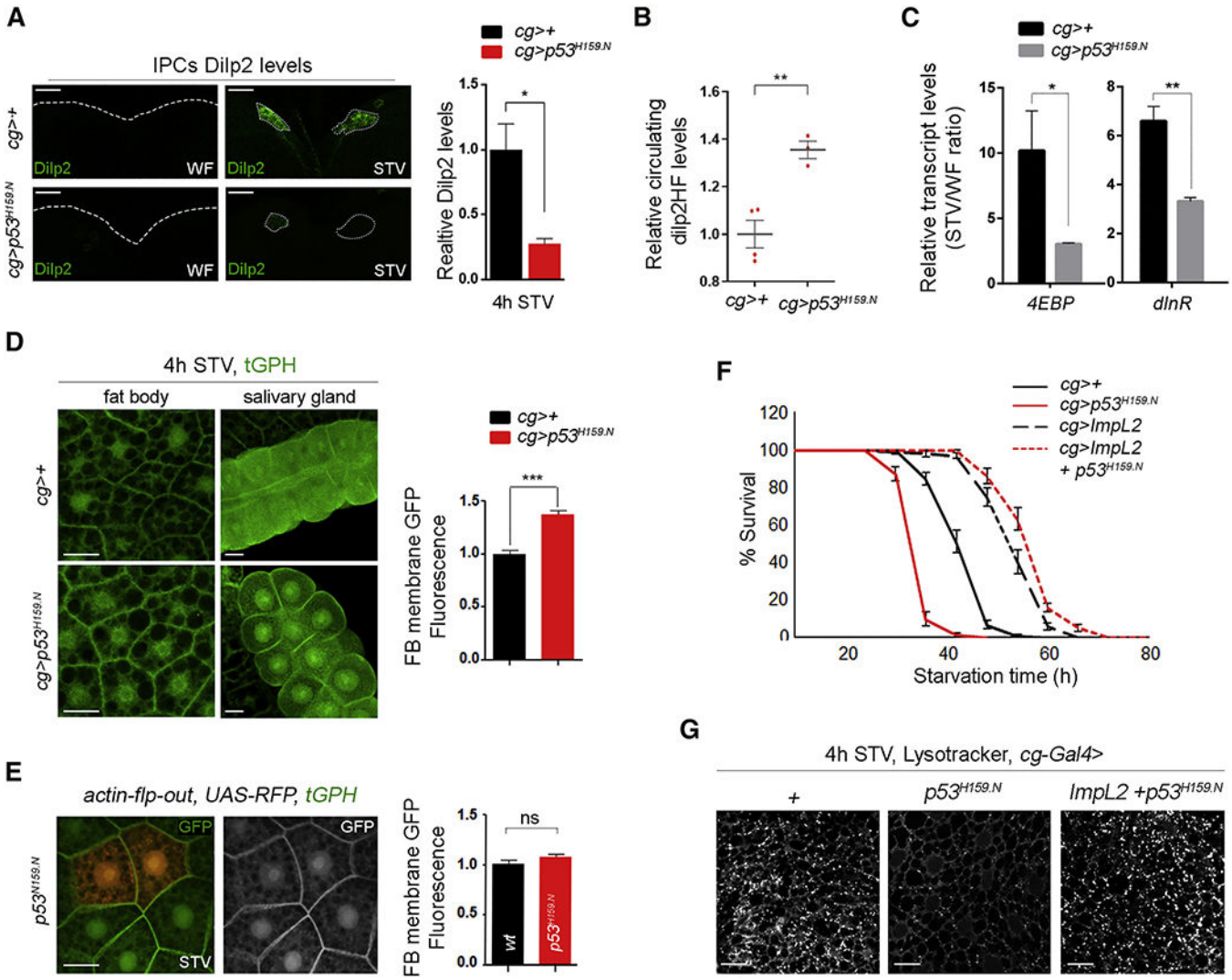

Fig. 4: Fat body Dmp53 activity regulates Dilp2 circulating levels and systemic insulin signaling

(A) Brain IPCs stained to visualize Dilp2 (green) protein levels in control (*cg>+)* and *cg>p53*$^{H159.N}$ larvae in WF and STV conditions (left). Relative Dilp2 levels showing reduced accumulation in starved *cg>p53*$^{H159.N}$ animals (right). n≥ 10 brains per genotype, representative of 3 independent experiments. (B) Immunoassays (ELISA) showing increased Dilp2-HF circulating levels in hemolymph of starved *cg>p53*$^{H159.N}$ compared to *cg>+* animals. (c) qRT-PCR showing *4EBP* and *dInR* transcript levels in the FB of *cg>+* and *cg>p53*$^{H159.N}$ animals subjected to WF or STV conditions. Results are expressed as fold induction respect to WF conditions. Three independent replicates were carried out for each sample. (D) FB and salivary gland cells labelled to visualize tGPH reporter (green) in *cg>+* and *cg>p53*$^{H159.N}$ animals in STV. Quantification of relative membrane-GFP fluorescence intensity in the FB (right). n≥ 40 for 3 independent experiments. (E) Starved FB cells expressing *Dmp53*$^{H159.N}$ (marked by the expression of RFP, in red) showed similar tGPH levels (in green or white) than neighboring wild-type cells. Relative tGPH levels between control and *Dmp53*$^{H159.N}$ expressing cells are shown (right). n≥ 10 for 3 independent experiments. (F) Survival rates to nutrient deprivation of adult flies (males) expressing

the indicated transgenes under *cg*-Gal4 control. ImpL2 overexpression totally reverted the reduced survival rates of *cg>p53$^{H159.N}$* flies upon starvation. See Table S1 for n, p, median, and maximum survival values. (G) Lysotracker staining showing that reduced autophagy induction observed in starved *cg>p53$^{H159.N}$* larvae was largely rescued when co-expressing ImpL2.

Mean ± SEM. ***p<0.001; **p<0.01; *p<0.05. Scale bars, 25 μm.

See also Figure S4 and Table S1.

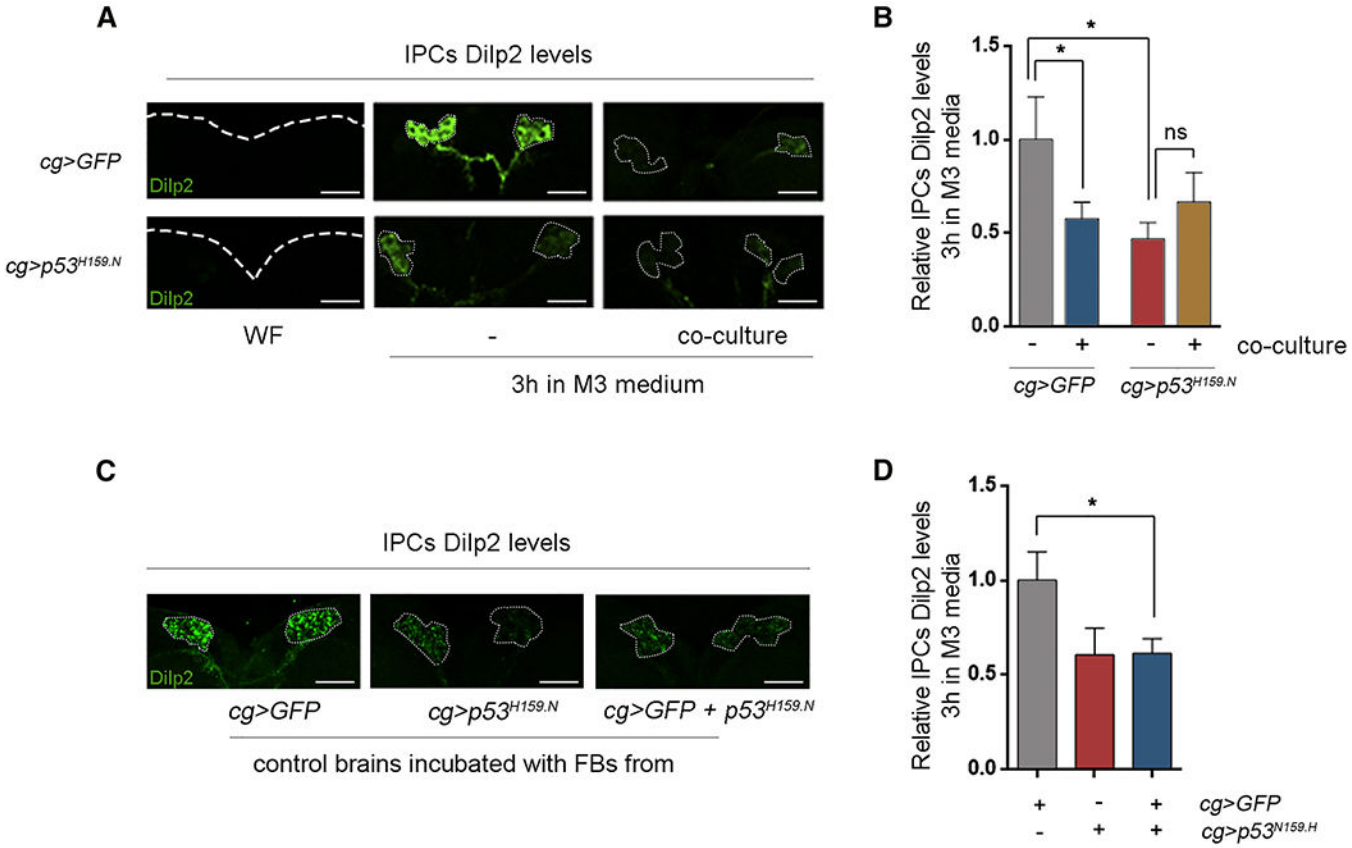

Fig. 5: Fat body Dmp53 remotely controls Dilp2 secretion upon starvation

Brain IPCs stained to visualize Dilp2 protein levels in *ex vivo* experiments. (A) Inverted larvae from control (*cg>GFP)* and *cg>p53*$^{H159.N}$ animals were incubated individually (middle panel) or together (co-culture; right panel) in M3 medium for 3 h and stained to visualize Dilp2 (green) protein levels. Whereas *cg>GFP* or *cg>p53*$^{H159.N}$ inverted larvae showed high and low Dilp2 accumulation levels when incubated individually, *cg>GFP* animals showed reduced IPCs Dilp2 levels when co-culture with *cg>p53*$^{H159.N}$ inverted larvae. Dilp2 protein levels in WF conditions are shown as controls (left panel). (C) Dissected brains from early L3 larvae were cultured in M3 insect medium in the presence or absence of fat bodies from control (*cg>GFP)* or *cg>p53*$^{H159.N}$ animals. Whereas control brains incubated *ex vivo* with *cg>GFP* fat bodies showed high Dilp2 accumulation levels, it showed reduced IPCs Dilp2 levels when incubated with fat bodies from *cg>p53*$^{H159.N}$ animals. (B, D) Quantification of relative IPCs Dilp2 fluorescence intensity from experiments shown in A and C, respectively. n= 6-8 (B) and n= 5 (D) for 2 independent experiment.

Mean ± SEM. *p<0.05; ns: not significant. Scale bars, 25 μm.

See also Figure S5.

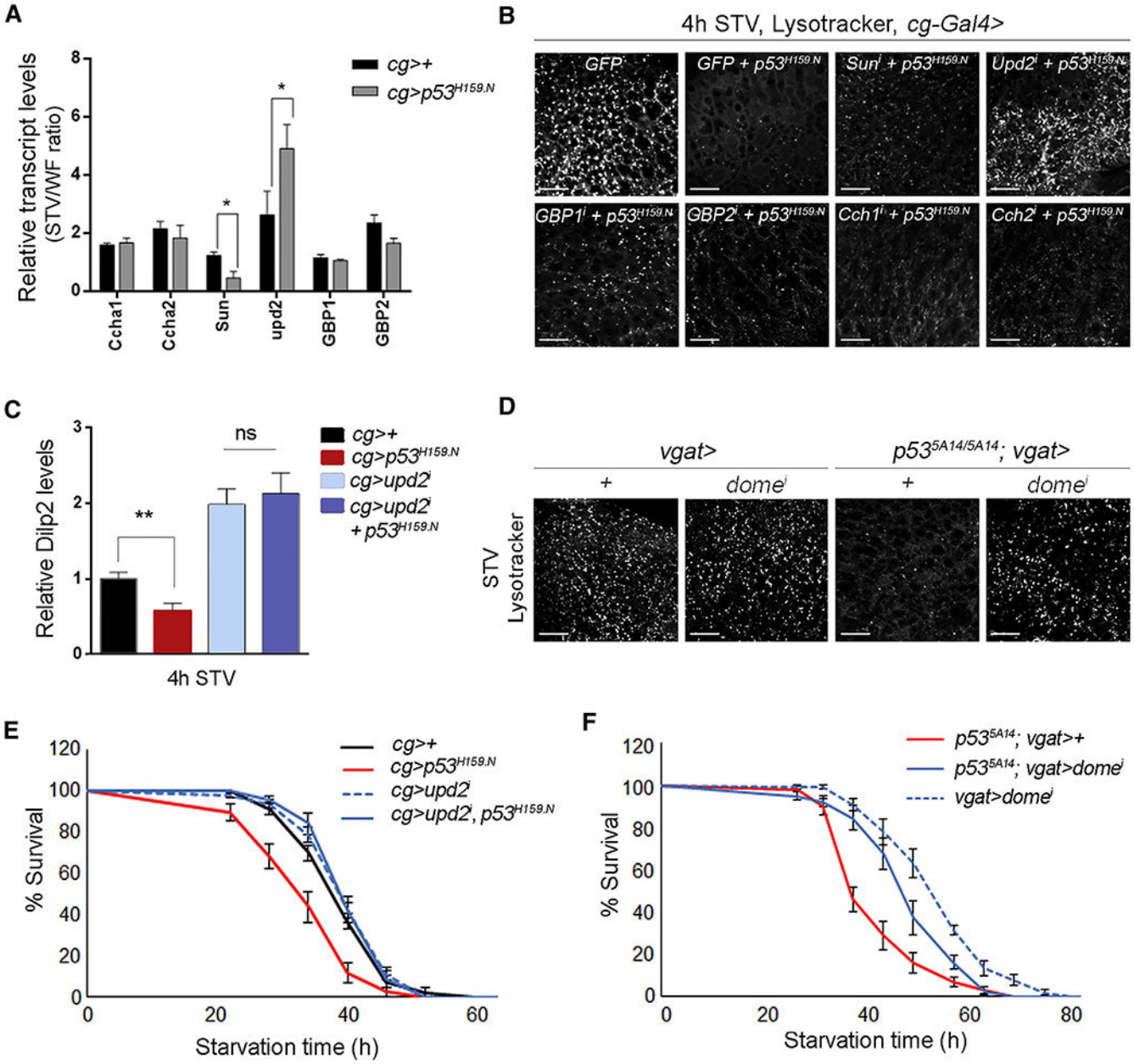

Fig. 6: Starvation-induced Dmp53 activation regulates Upd2 levels, autophagy induction and survival rates

(A) qRT-PCR showing mRNA levels of indicated genes in control (*cg>+)* and *cg>p53*$^{H159.N}$ larvae in WF and STV conditions. Results are expressed as fold induction respect to WF conditions. Three independent replicates were carried out for each sample. (B) Lysotracker staining in the FB of starved larvae expressing GFP (control) or *Dmp53*$^{H159.N}$ along with the indicated transgenes under cg-Gal4 control. (C) Quantification of mean Dilp2 fluorescence intensity in the IPCs of starved larvae expressing the indicated transgenes in the FB under *cg*-Gal4 control. n≥ 10 brains per genotype, representative of 2 independent experiment. (D) Lysotracker staining in the FB of starved larvae expressing *dome*^{i} in GABAergic neurons by using the *vgat*-Gal4 driver in either wild-type or *p53*^{5A14} mutant

background. (E-F) Survival rates to nutrient deprivation of adult flies (females) expressing the indicated transgenes under the control of cg-Gal4 (E) or *vgat*-Gal4 (F) drivers. Inhibiting *Upd2* expression in the FB totally reverted the reduced survival rates of $cg>p53^{H159.N}$ flies upon starvation (E), and blocking JAK/STAT signaling in GABAergic neurons strongly rescued the reduced survival rates of $p53^{5A14}$ mutant flies (F). See Table S1 for n, p, median, and maximum survival values.

Mean ± SEM. **p<0.01; *p<0.05; ns: not significant. Scale bars, 25 μm.

See also Figure S6 and Table S1.

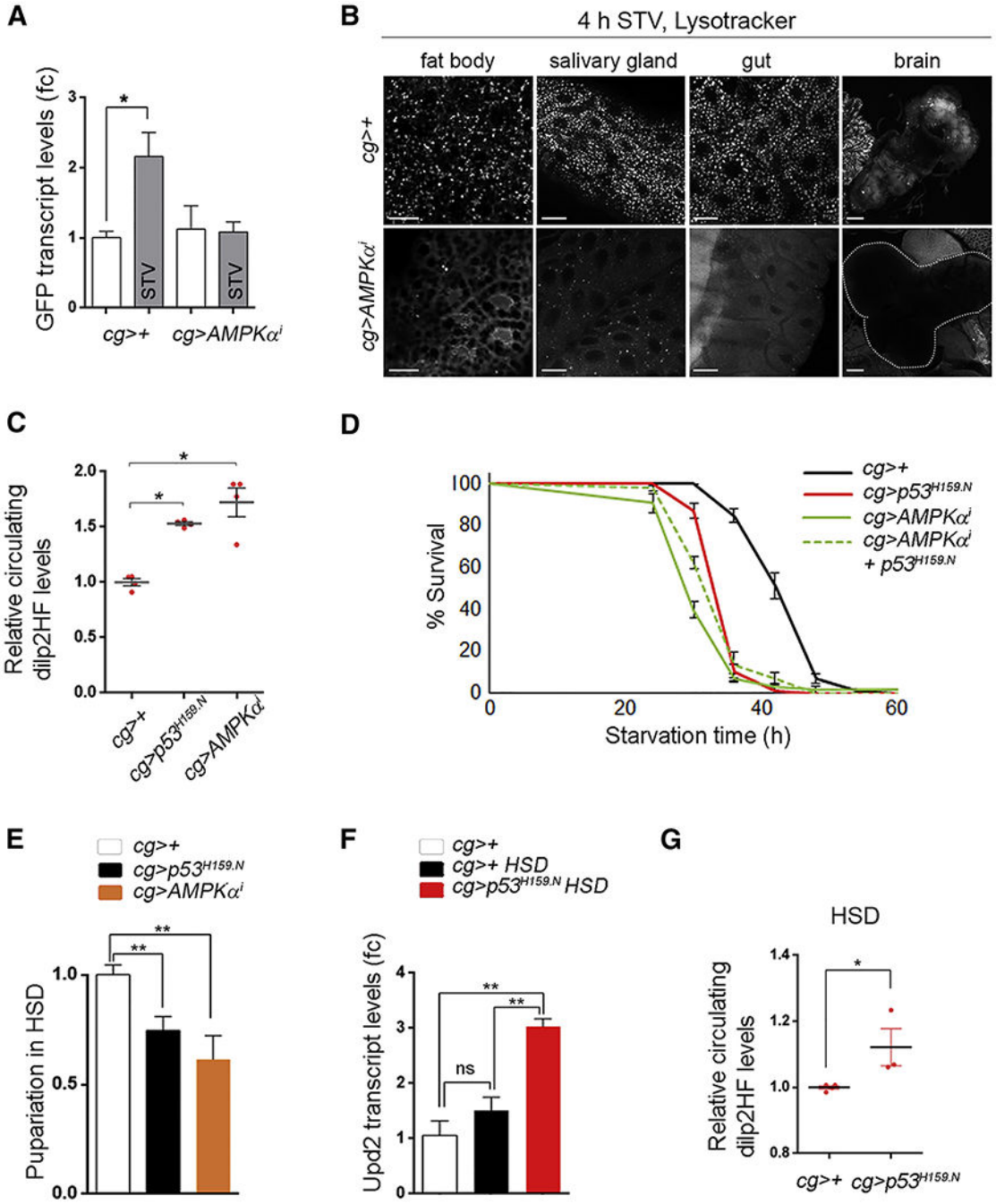

Fig. 7: Effect of fat body AMPK-Dmp53 axis in controlling insulin signaling, autophagy and survival under nutrient stress

(A) qRT-PCR showing *gfp* mRNA levels in the FB of control (*cg>+*) and *cg>AMPKα^i* larvae bearing $p53^{RE}$-GFP and subjected to WF or STV conditions. Results are expressed as fold induction respect to control WF animals. Three independent replicates were carried out for each sample. (B) Lysotracker staining in the FB, salivary gland, intestine and brain of starved *cg>+* and *cg>AMPKα^i* animals. (C) Immunoassays (ELISA) showing increased Dilp2-HF circulating levels in hemolymph of starved *cg>p53^H159.N* or *cg>AMPKα^i* larvae. Results are normalized to control animals in STV conditions. (D) Survival rates to nutrient

deprivation of adult flies (males) expressing the indicated transgenes in the FB under cg-Gal4 control. Co-expression of *Dmp53*$^{H159.N}$ and AMPKα^{i} showed similar survival rates as expression of each transgene individually. See Table S1 for n, p, median, and maximum survival values. (E) Number of individuals entering pupariation from control, *cg>p53*$^{H159.N}$ or *cg>AMPKα*^{i} animals raised immediately after hatching in HSD. Data were represented as a ratio of HSD-fed control animals. (F) qRT-PCR showing increased *upd2* transcript levels in HSD-fed larvae expressing *Dmp53*$^{H159.N}$ under cg-Gal4 control. Results are expressed as fold induction respect to control WF animals. Three independent replicates were carried out for each sample. (G) Immunoassays (ELISA) showing increased Dilp2-HF circulating levels in hemolymph of HSD-fed animals from *cg>p53*$^{H159.N}$. Results are normalized to control animals in HSD.

Mean ± SEM. *p<0.05;**p<0.01. Scale bars, 25 μm.

See also Figure S7 and Table S1.

KEY RESOURCES TABLE

REAGENT or RESOURCE	SOURCE	IDENTIFIER
Antibodies		
Rabbit polyclonal anti-β-galactosidase	Invitrogen	Cat#A11132
Mouse monoclonal anti-GFP	Developmental Studies Hybridoma Bank	Cat#12A6
Rat polyclonal anti-Dilp2	Géminard et al., 2009	N/A
Rabbit anti-phospho-Drosophila S6 Kinase	Cell Signaling	Cat#9209
Mouse monoclonal anti-actin	Developmental Studies Hybridoma Bank	JLA20
Mouse monoclonal anti-FLAG	Sigma	Cat#F1804
Anti-HA-Peroxidase	Roche	Cat#12013819001
Bacterial and Virus Strains		
Biological Samples		
Chemicals, Peptides, and Recombinant Proteins		
Lysotracker Green	ThermoFisher	Cat#L7526
Rapamycin	LC Labs	Cat#R5000
Critical Commercial Assays		
1-Step Ultra TMB-ELISA Substrate	ThermoFisher	Cat#34029
Amyloglucosidase	Sigma	Cat#A7420
Glucose (GO) Assay Kit	Sigma	Cat#GAGO-20
TRIZOL RNA Isolation Reagent	Invitrogen	Cat#15596026
Halt Protease Inhibitor Cocktail	ThermoFisher	Cat#87785
Cell lysis buffer	Cell Signalling	Cat #9803
SuperSignal™ West Pico PLUS Chemiluminescent Substrate	ThermoFisher	Cat#34580
Deposited Data		
Experimental Models: Cell Lines		
Experimental Models: Organisms/Strains		
cg-Gal4	Bloomington Drosophila Stock Center	BDSC:7011
ppl-Gal4	Bloomington Drosophila Stock Center	BDSC:58768
R4-Gal4	Bloomington Drosophila Stock Center	BDSC:33832
Isp2-Gal4	Bloomington Drosophila Stock Center	BDSC:6357
vgat-Gal4	Bloomington Drosophila Stock Center	BDSC:58980
fkh-Gal4	Bloomington Drosophila Stock Center	BDSC:78061
elav-Gal4	Bloomington Drosophila Stock Center	BDSC: 8765
$dmp53^{ns}$	Bloomington Drosophila Stock Center	BDSC: 23283
$dmp53^{5A14}$	Bloomington Drosophila Stock Center	BDSC: 6815

REAGENT or RESOURCE	SOURCE	IDENTIFIER
UAS-Dmp53^{H159N}	Bloomington Drosophila Stock Center	BDSC: 8420
UAS-Dmp53^{R155H}	Bloomington Drosophila Stock Center	BDSC: 8419
GUS-Dmp53^{259H}	Bloomington Drosophila Stock Center	BDSC: 6582
UAS-Dmp53^{RNAi}	Bloomington Drosophila Stock Center	BDSC: 29351
UAS-AMPKα^{RNAi}	Bloomington Drosophila Stock Center	BDSC: 57785
UAS-sun^{RNAi}	Vienna Drosophila Resource Center	VDRC: 23685
UAS-upd2^{RNAi}	Bloomington Drosophila Stock Center	BDSC: 33949
UAS-ccha1^{RNAi}	Bloomington Drosophila Stock Center	BDSC: 57562
UAS-ccha2^{RNAi}	Bloomington Drosophila Stock Center	BDSC: 57183
UAS-gbp1^{RNAi}	Vienna Drosophila Resource Center	VDRC: 15512
UAS-gbp2^{RNAi}	Vienna Drosophila Resource Center	VDRC: 330018
UAS-dome^{RNAi}	Bloomington Drosophila Stock Center	BDSC: 53890
tGPH	Britton et at, 2002	N/A
unk-lacZ	Tiebe et al., 2015	N/A
Dilp2-HF	Park et al., 2014	N/A
p53^{RE}-GFP	Lu et al., 2010	N/A
hsFlp; UAS-Dicer2; R4-Cherry-atg8, act>y+>Gal4, UAS-GFP	Arsham and Neufeld, 2009	N/A
UAS-mCherry-atg8a	Yu-Yun Chang and Thomas P. Neufeld, 2009	N/A
Oligonucleotides		
Oligos used in this study are listed in Table S2		N/A
Recombinant DNA		
Software and Algorithms		
Prism	Graph Pad	https://www.graphpad.com/scientific-software/prism/
Adobe Photoshop CS5	Adobe	www.adobe.com/uk/products/photoshop.html
Leica Confocal Software	Leica	www.leica-microsystems.com/products/microscopesoftware/
Fiji	Schindelin et al., 2012	imagej.nih.gov/ij/
Other		